

1 **Bayesian Inference and Predictive Performance of Soil Respiration Models in the Presence**
2 **of Model Discrepancy**

3
4 Ahmed S. Elshall^{1,2}, Ming Ye^{3,*}, Guo-Yue Niu^{4,5} and Greg A. Barron-Gafford^{4,6}

5
6 ¹ Department of Earth Sciences, University of Hawai‘i Manoa, Honolulu, Hawaii, USA

7 ² Water Resources Research Center, University of Hawai‘i Manoa, Honolulu, Hawaii, USA

8 ³ Department of Earth, Ocean, and Atmospheric Science, Florida State University, Tallahassee,
9 Florida, USA

10 ⁴ Biosphere 2, University of Arizona, Tucson, Arizona, USA

11 ⁵ Department of Hydrology and Water Resources, University of Arizona, Tucson, Arizona, USA

12 ⁶ School of Geography and Development, University of Arizona, Tucson, Arizona, USA

13
14
15 *Corresponding Author: Ming Ye, Telephone: (850) 644-4587, Email: mye@fsu.edu

16
17
18 Submitted for publication in Geoscientific Model Development

19
20 April, 2019

47
48
49
50
51
52
53
54
55
56
57
58
59
60
61
62
63
64
65
66
67
68
69
70
71

Key Points

- (1) Bayesian inference and prediction are useful to evaluate multiple soil respiration models with different levels of model complexity.
- (2) Data models used in Bayesian inference have substantial impacts on model parameter distributions and subsequently model predictions.
- (3) Using exponential power distribution and considering heteroscedasticity in data models improve Bayesian inference and prediction.

Keywords: Soil respiration, modeling, Bayesian, likelihood function, data model, autocorrelation, heteroscedasticity, skew exponential power distribution, cross-validation, scoring rule

72 **Abstract**

73 Bayesian inference of microbial soil respiration models is often based on the assumptions that the
74 residuals are independent (i.e. no temporal or spatial correlation), identically distributed (i.e.
75 Gaussian noise) and with constant variance (i.e. homoscedastic). In the presence of model
76 discrepancy, since no model is perfect, this study shows that these assumptions are generally
77 invalid in soil respiration modeling such that residuals have high temporal correlation, an
78 increasing variance with increasing magnitude of CO₂ efflux, and non-Gaussian distribution.
79 Relaxing these three assumptions stepwise results in eight data models. Data models are the basis
80 of formulating likelihood functions of Bayesian inference. This study presents a systematic and
81 comprehensive investigation of the impacts of data model selection on Bayesian inference and
82 predictive performance. We use three mechanistic soil respiration models with different levels of
83 model fidelity (i.e. model discrepancy) with respect to number of carbon pools and explicit
84 representations of soil moisture controls on carbon degradation, and accordingly have different
85 levels of model complexity with respect to the number of model parameters. The study shows data
86 models have substantial impacts on Bayesian inference and predictive performance of the soil
87 respiration models such that: (i) the level of complexity of the best model is generally justified by
88 the cross-validation results for different data models; (ii) not accounting for heteroscedasticity and
89 autocorrelation might not necessarily result in biased parameter estimates or predictions, but will
90 definitely underestimate uncertainty; (iii) using a non-Gaussian data model improves the parameter
91 estimates and the predictive performance; and (iv) separate accounting for autocorrelation or joint
92 inversion of correlation and heteroscedasticity can be problematic and requires special treatment.
93 Although the conclusions of this study are empirical, the analysis may provide insights for
94 selecting appropriate data models for soil respiration modeling.

95 **1 Introduction**

96 Developing accurate soil respiration models is important for realistic projection of global
97 carbon [C] cycle, as global soils store 2,300Pg carbon, an amount more than 3 times that of the
98 atmosphere (Schmidt et al., 2011) and release 60–75 Pg C/yr, about 7 times more CO₂ to the
99 atmosphere than all human-caused emissions (Le Quéré et al., 2014). The major work on soil
100 respiration modeling has been focused on advancing knowledge about model inputs and
101 calibration data (e.g. Janssens et al., 2003; Peters et al., 2007; Scott et al., 2009; Barron-Gafford et
102 al., 2011; Hilton et al., 2014) and on developing more advanced models for better representing
103 soil microbial processes (e.g. Schimel and Weintraub, 2003; Allison et al., 2010; Davidson et al.,
104 2011; Wieder et al., 2013, 2015; Xu et al., 2014; Zhang et al., 2014) . Integration of data and
105 models is indispensable for improving predictability of the terrestrial carbon cycle, and statistical
106 modeling is a vital tool for the model-data integration (Luo et al., 2011, 2014; Wieder et al., 2015).
107 In addition, use of state-of-the-art statistical methods is necessary to accurately quantify
108 uncertainty in parameters and structures of soil respiration models for improvement and practical
109 uses of the models (Katz et al., 2013). A data model that is also known as a residuals model or an
110 error model is used to characterize residuals (i.e., the difference between data and corresponding
111 model simulations). While a large number of data models have been used (e.g. Elshall et al., 2018;
112 Scholz et al., 2018) to our knowledge comprehensive and systematic evaluation of data models for
113 soil respiration modeling has not been reported in literature.

114 The objectives of this study are to evaluate the impacts of data models on Bayesian inference
115 and predictive performance of three mechanistic soil respiration models, and to use the evaluation
116 results to make broader recommendations. The three models were developed by Zhang et al. (2014)
117 to simulate the Birch effect (the peak soil microbial respiration pulses in response to episodic

118 rainfall pulses) at a site scale and a short temporal scale; understanding the Birch effect is important
119 for gaining mechanistic understanding of CO₂ efflux production (Högberg and Read, 2006; Vargas
120 et al., 2011). The models of Zhang et al. (2014) are based on an existing four-carbon pool model,
121 but have additional carbon pools and/or explicit representations of soil moisture controls on carbon
122 degradation and microbial uptake rates. The models were calibrated, and Bayesian model selection
123 was used to select the best model (Zhang et al., 2014). However, this effort was based on a single
124 data model. It is unknown whether the best model still remains the best (in terms of reproducing
125 the both calibration data and the cross-validation data) if a different data model is used. In addition,
126 since predictive performance of the models was not evaluated in Zhang et al. (2014), it is unknown
127 whether the best model will give the best predictions. These two questions are addressed in this
128 study by considering eight data models and by evaluating predictive performance in a manner of
129 cross-validation. The top two models (also the two most high fidelity models) ranked by Zhang et
130 al. (2014) are considered in this study, and the worst model (also the low fidelity model) is also
131 considered in this study for comparison. We use the terms model fidelity and model discrepancy
132 interchangeably. Model fidelity refers to the degree of realism of representing our scientific
133 knowledge with respect to the real world system. That is a high fidelity model has less discrepancy.
134 Evaluating predictive performance for the three models with different degrees of fidelity provides
135 more insights than a single model.

136 Bayesian inference in general uses the Bayes' theorem to update the prior distributions of
137 model parameters to posterior parameter distributions given a likelihood function of data. The
138 mathematical formulation of the (formal and informal) likelihood function requires a probabilistic
139 data model that however is intrinsically unknown due to unknown errors in all model components
140 such as model structures, parameters, and driving forces. Bayesian inference of soil respiration

141 models often adopts the assumption of independent, normally distributed and homoscedastic
142 residuals (e.g. Ahrens et al., 2014; Bagnara et al., 2015, 2018; Barr et al., 2013; Barron-gafford et
143 al., 2014; Braakhekke et al., 2014; Braswell et al., 2015; Correia et al., 2012; Du et al., 2015, 2017;
144 Hararuk et al., 2014; Hashimoto et al., 2011; He et al., 2018; Klemedtsson et al., 2008; Menichetti
145 et al., 2016; Raich et al., 2002; Ren et al., 2013; Richardson and Hollinger, 2005; Steinacher and
146 Joos, 2016; Tucker et al., 2014; Tuomi et al., 2008; Xu et al., 2006; Yeluripati et al., 2009; Yuan
147 et al., 2012, 2016; Zhang et al., 2014; Zhou et al., 2010). These assumptions are conveniently
148 adopted to satisfy the requirement of using an unknown probability model in Bayesian statistics,
149 which is called “a basic dilemma” by (Box and Tiao, 1992).

150 Postulating the data models is always based on assumptions about residual statistics, and the
151 most widely used assumptions are paired as follows: (i) independent vs. correlated residuals, (ii)
152 homoscedastic vs. heteroscedastic residuals, and (iii) Gaussian vs. non-Gaussian residuals. For soil
153 respiration modeling few studies have relaxed the non-correlation assumption(e.g. Cable et al.,
154 2008, 2011; Li et al., 2016b), the homoscedasticity assumption (e.g. Berryman et al., 2018; Elshall
155 et al., 2018; Ogle et al., 2016; Tucker et al., 2013), and the non-Gaussian and homoscedasticity
156 assumptions (e.g. Elshall et al., 2018; Ishikura et al., 2017; Kim et al., 2014). The recent study of
157 Scholz et al. (2018) relaxed these three assumptions using the generalized likelihood function
158 developed by Schoups and Vrugt (2010). However, few studies have focused on investigating
159 appropriateness and impact of these assumptions for soil respiration modeling, by relaxing the
160 independent residuals assumption (Ricciuto et al., 2011) and the Gaussian residuals assumption
161 (Ricciuto et al., 2011; van Wijk et al., 2008). By relaxing these three assumptions stepwise
162 resulting in eight data models, to our knowledge this is the first study that systematically evaluates
163 the impact of data model selection on Bayesian inference and predictive performance of soil

164 respiration modeling. In addition, to our knowledge this is the first soil respiration modeling study
165 that investigates the impact of data models in relation to model fidelity.

166 Relaxing these three assumption results in eight data models, which are shown in details in
167 Section 2. For example, combining the assumptions of independent, homoscedastic, and Gaussian
168 residuals leads to the standard least squares data model. This model is the simplest one among the
169 eight data models, since it requires only one parameter, i.e., the constant variance of the Gaussian
170 distribution. Note that there is a difference between the soil respiration model parameters and the
171 data model parameters. They technically can be jointly estimated, but one arises from assumptions
172 about soil respiration processes, and the other from assumptions about the residuals. Relaxing the
173 homoscedastic assumption to heteroscedastic gives the weighted least squares data model. It is
174 more complex because it has extra parameters to account for multiple variances for multiple data.
175 Whenever one or combinations of the three assumptions (independence, homoscedasticity, and
176 normality) are relaxed, the resulting data models become more complex and require more
177 parameters. Such systematic evaluation of data models (McInerney et al., 2017; Smith et al. 2010b,
178 2015) is necessary to evaluate appropriateness of residuals assumptions and their impacts on
179 Bayesian inference.

180 The assumptions of heteroscedastic, correlated, and non-Gaussian residuals are accounted for
181 by using the method of Schoups and Vrugt (2010) in the following procedure: (i) the correlation
182 is removed from the residuals by using an autoregressive model; (ii) the resulting residuals are
183 normalized by a linear model of variance; and (iii) the normalized residuals are characterized by
184 using the skew exponential power distribution. The data model parameters (i.e., coefficients of the
185 autoregressive model, the linear variance model, and the skew exponential power distribution) are
186 not specified by users, but estimated together with soil respiration model parameters during the

187 Bayesian inference. The skew exponential power distribution is general in that by adjusting the
188 values of its kurtosis and skewness parameters the distribution can produce other distributions such
189 as the Laplace distribution (van Wijk et al., 2008; Ricciuto et al., 2011) and other distributions
190 through using an exponential model with different kurtosis parameters (Tang and Zhuang, 2009).
191 It is worth pointing out that there exist other methods to account for the three assumptions. Evin
192 et al. (2013) suggested accounting for residual heteroscedasticity before accounting for residual
193 autocorrelation. Lu et al. (2013) developed an iterative two-stage procedure to separately estimate
194 physical model parameters and data model parameters. Evin et al. (2014) developed a similar
195 procedure to first estimate model parameters and then estimate heteroscedasticity and
196 autocorrelation parameters. While this study uses the method of Schoups and Vrugt (2010),
197 exploring other methods is warranted in future studies.

198 After investigating the impacts of the data models on Bayesian inference, this study evaluates
199 the impacts of the data models on predictive performance of the three soil respiration models.
200 Using random samples generated during the Bayesian inference, a prediction ensemble is produced
201 for each soil respiration model. The ensemble is used to evaluate predictive performance of the
202 models in a stochastic sense by estimating to what extent the models can predict future events. The
203 evaluation in this study is done in a cross-validation manner by splitting the dataset of CO₂ efflux
204 into two parts for Bayesian inference and cross-validation, respectively. The evaluation of
205 predictive performance is important because different data models may give different parameter
206 distributions and accordingly different predictive performance. For example, the study of van Wijk
207 et al. (2008) concluded that the choice of the residual function is crucial to achieve accurate model
208 prediction and parameter estimation. Shi et al. (2014) showed that the posterior parameter
209 distributions and predictive performance given by two data models (weighted least square and

210 skew exponential power distribution after removing heteroscedasticity and autocorrelation) are
211 dramatically different, and a definitive conclusion was drawn that one data model is better than
212 the other. The evaluation of predictive analysis is conducted for the following two cases: (1) the
213 prediction ensemble is generated by random samples of the soil respiration models only (i.e.
214 credible interval), and (2) the prediction ensemble is generated by random samples of not only the
215 soil respiration models but also the data models (i.e. predictive interval). The two cases lead to
216 different conclusions about the predictive performance. It is expected that the evaluation of
217 predictive performance conducted in this study can help select the most appropriate data model to
218 achieve optimal model predictions.

219 The remainder of the paper is organized as follows. Section 2 starts with a description of the
220 evolving data models and their corresponding likelihood functions used in Bayesian inference,
221 followed by a brief summary of the three soil respiration models. The results of Bayesian inference
222 are discussed in Section 3 and Section 4, addressing the data model implications on parameter
223 estimation and predictive performance, respectively. Section 5 summarizes the key findings and
224 limitations of this study, and provides recommendations for approaching data model selection.

225 **2 Methodology**

226 This section starts with a description of the eight data models that account for the three pairs
227 of assumptions about residuals in a stepwise manner in Section 2.1. The data models are used to
228 build the likelihood functions used in Section 2.2 for Bayesian inference. The three soil respiration
229 models and observations of CO₂ efflux are described in Sections 2.3 and 2.4, respectively. Metrics
230 for evaluating predictive performance are presented in Section 2.5.

231

232 2.1 Data models

233 This study considers eight evolving data models starting from a data model that assumes
234 independent, homoscedastic, and Gaussian residuals to a data model that relaxes all the three
235 assumptions. The eight data models are based on the generic normalized residual,

$$236 \quad a_t = \frac{\varepsilon_t}{\sigma_t} \quad a_t \sim X, \quad (1)$$

237 where $\varepsilon_t = d_t - Y_t$ is the residual (the difference between data d_t and its corresponding model
238 simulation Y_t) at time or location t ; σ_t is the standard deviation of the residual; and X is the
239 probability density function (PDF) of a_t . The eight data models are formulated with different forms
240 of ε_t , σ_t , and X . The standard least square (SLS) data model is

$$241 \quad a_t = \frac{\varepsilon_t}{\sigma_0} \quad a_t \sim N(0,1), \quad (2)$$

242 where $\sigma_t = \sigma_0$ is a constant for all the data (i.e., homoscedasticity), and X is the standard normal
243 distribution, $N(0,1)$. The unknown parameter σ_0 is estimated jointly with unknown physical
244 model parameters. If σ_t is not a constant (i.e., heteroscedastic), SLS becomes the weighted least
245 squared (WLS) data model. While heteroscedasticity can be accounted for through residuals
246 transformation (e.g. Thiemann et al., 200; Smith et al., 2010b) or other similar approaches (Gragne
247 et al., 2015) , a linear heteroscedastic model $\sigma_t = \sigma_0 + \sigma_1 Y_t$ is assumed here by following the
248 studies of Thyer et al. (2009), Schoups and Vrugt (2010), and Evin et al. (2013, 2014). With the
249 linear model, there is no need to estimate σ_t for each data. Instead, σ_t is calculated by estimating
250 only two parameters, σ_0 and σ_1 . The WSL data model is written as

$$251 \quad a_t = \frac{\varepsilon_t}{\sigma_0 + \sigma_1 Y_t} \quad a_t \sim N(0,1). \quad (3)$$

252 The two unknown parameters σ_0 and σ_1 are estimated jointly with unknown physical model
 253 parameters. The linear model assigns smaller weight to the data with larger simulation, Y_t . If the
 254 simulation is small and $\sigma_0 \gg \sigma_1 Y_t$, the weight becomes constant for all data. Both SLS and WLS
 255 assume that a_t is independently and identically distributed.

256 It is not uncommon that residuals are correlated in space and time, due to propagation of
 257 measurement errors (Tiedeman and Green, 2013) and model structure errors (Evin et al., 2014;
 258 Kavetski et al., 2013; Lu et al., 2013). The temporal correlation that occurs in the numerical
 259 example of this study can be accounted for by using a p -order autoregressive model. This leads to
 260 the data model of standard least square with autocorrelation (SLS-AC),

$$261 \quad a_t = \frac{\varepsilon_t - \sum_{i=1}^p \phi_i \varepsilon_{t-i}}{\sigma_0} \quad a_t \sim N(0,1) \quad (4)$$

262 where p is the order of autocorrelation, and ϕ_i is an autocorrelation coefficient. The unknown ϕ_i
 263 and σ_0 are estimated together with unknown model parameters. By extending the concept of
 264 correlated residuals to WLS leads to the weight least square with autocorrelation (WLS-AC),

$$265 \quad a_t = \frac{\varepsilon_t - \sum_{i=1}^p \phi_i \varepsilon_{t-i}}{\sigma_0 + \sigma_1 Y_t} \quad a_t \sim N(0,1) \quad (5)$$

266 The unknown parameters of σ_0 , σ_1 , and ϕ_i are estimated jointly with physical model
 267 parameters. Equations (2) – (5) assume that the residuals are Gaussian.

268 The next four data models are similar to the previous four models except that the standard
 269 normal distribution of a_t is replaced by the skew exponential power distribution, $SEP(0,1,\xi,\beta)$,
 270 with zero mean and unit standard deviation (Schoups and Vrugt, 2010)

271
$$p(a_t | \xi, \beta) = \frac{2\sigma_\xi}{\xi + \xi^{-1}} \omega_\beta \exp\left[-c_\beta |a_{\xi,t}|^{2/(1+\beta)}\right], \quad (6)$$

272 where ξ is skewness, β is kurtosis, $a_{\xi,t} = (\mu_\xi + \sigma_\xi a_t) / \xi^{\text{sign}(\mu_\xi + \sigma_\xi a_t)}$, $\mu_\xi = M(\xi - \xi^{-1})$,

273
$$\omega_\beta = \frac{\Gamma^{1/2}[3(1+\beta)/2]}{(1+\beta)\Gamma^{3/2}[(1+\beta)/2]}, \quad \sigma_\xi = \sqrt{(1-M^2)(\xi^2 + \xi^{-2}) + 2M^2 - 1},$$

274
$$M = \frac{\Gamma[1+\beta]}{\Gamma^{1/2}[3(1+\beta)/2]\Gamma^{1/2}[(1+\beta)/2]}, \text{ and } c_\beta = \left(\frac{\Gamma[3(1+\beta)/2]}{\Gamma[(1+\beta)/2]}\right)^{1/(1+\beta)}$$
 are derived variables of β and

275 ξ , and $\Gamma[\cdot]$ is the gamma function. The kurtosis parameter $\{\beta \in \mathbb{R} : -1 \leq \beta \leq 1\}$ determines the

276 peakness of the pdf such that the β values of -1, 0, and 1 give uniform, Gaussian and Laplace

277 distributions, respectively. The skewness parameter $\{\xi \in \mathbb{R} : 0.1 \leq \xi \leq 10\}$ determines the

278 skewness of the pdf such that the ξ values of 0.1, 1, and 10 give positively skewed, symmetric,

279 and negatively skewed distributions, respectively. Setting $\beta=0$ and $\xi=1$ leads to $\mu_\xi = 0, \sigma_\xi = 1$

280 , $\omega_\beta = 1/\sqrt{2\pi}$, $c_\beta = 1/2$ and $a_{\xi,t} = a_t$, and the skew exponential power distribution

281 $SEP(0,1,\xi=1,\beta=0)$ becomes the standard normal distribution,

282
$$p(a_t | \xi=1, \beta=0) = \frac{1}{\sqrt{2\pi}} \exp\left[-\frac{1}{2}(a_t)^2\right]. \quad (7)$$

283 which is the data model of SLS in equation (2).

284 Replacing $a_t \sim N(0,1)$ with $a_t \sim SEP(0,1,\xi,\beta)$ in equations (2)–(5) leads to the data models

285 SEP, WSEP, SEP-AC, and WSEP-AC as follows,

286
$$a_t = \frac{\varepsilon_t}{\sigma_0} \quad a_t \sim SEP(0,1,\xi,\beta) \quad (8)$$

287
$$a_t = \frac{\varepsilon_t}{\sigma_0 + \sigma_1 Y_t} \quad a_t \sim SEP(0,1,\xi,\beta). \quad (9)$$

288
$$a_t = \frac{\varepsilon_t - \sum_{i=1}^p \phi_i \varepsilon_{t-i}}{\sigma_0} \quad a_t \sim SEP(0, 1, \xi, \beta) \quad (10)$$

289
$$a_t = \frac{\varepsilon_t - \sum_{i=1}^p \phi_i \varepsilon_{t-i}}{\sigma_0 + \sigma_1 Y_t} \quad a_t \sim SEP(0, 1, \xi, \beta) \quad (11)$$

290 In comparison with the Gaussian data models, the SEP-based data models have two more
 291 parameters (ξ and β) to be estimated jointly with physical model parameters. Data model WSEP-
 292 AC, which is known as the generalized likelihood function, is the most commonly used SEP-based
 293 data model (e.g. Vrugt and Ter Braak, 2011; Hublart et al., 2016; Scholz et al., 2018). A summary
 294 table of the eight data models with corresponding parameters is provided in the supplementary
 295 materials.

296 2.2 Bayesian inference and likelihood functions

297 Consider a Bayesian inference problem for a nonlinear model, f , used to simulate state
 298 variables (e.g., CO₂ efflux), $\mathbf{d} = \mathbf{Y}(\boldsymbol{\theta}) + \boldsymbol{\varepsilon}$, where \mathbf{d} is a vector of data, $\boldsymbol{\theta}$ is a vector of model
 299 parameters, and $\boldsymbol{\varepsilon}$ is a vector of residuals that may include errors in data, model parameters, and
 300 model structures. The goal of Bayesian inference is to estimate the posterior distributions, $p(\boldsymbol{\theta}|\mathbf{d})$,
 301 of model parameters, $\boldsymbol{\theta}$, given data, \mathbf{d} , using Bayes' theorem (Box and Tiao, 1992)

302
$$p(\boldsymbol{\theta}|\mathbf{d}) = \frac{p(\mathbf{d}|\boldsymbol{\theta})p(\boldsymbol{\theta})}{\int p(\mathbf{d}|\boldsymbol{\theta})p(\boldsymbol{\theta})d\boldsymbol{\theta}} \quad (12)$$

303 where $p(\boldsymbol{\theta})$ is the prior distribution, and $p(\mathbf{d}|\boldsymbol{\theta})$ is the likelihood function to measure goodness-of-
 304 fit between model simulations, $\mathbf{Y}(\boldsymbol{\theta})$, and data, \mathbf{d} . The prior distribution can be obtained from data
 305 of previous studies (e.g. Elshall and Tsai, 2014) or expert judgment. When prior information is
 306 lacking, a common practice is to assume uniform distributions with relatively large parameter
 307 ranges so that the prior distributions do not affect the estimation of posterior distributions.

308 The data models above can be used to construct the likelihood functions. For the Gaussian data
 309 models given in equations (2) – (5), the corresponding Gaussian likelihood functions are
 310 straightforward, and an example is equation (7). For the SEP data models, the corresponding
 311 likelihood that is called generalized likelihood function is (Schoups and Vrugt, 2010)

$$312 \quad p(\mathbf{d} | \boldsymbol{\theta}) = p(\boldsymbol{\varepsilon}_t | \boldsymbol{\theta}) = \prod_{t=1}^n \sigma_t^{-1} \frac{2\sigma_\xi}{\xi + \xi^{-1}} \omega_\beta \exp\left(-c_\beta |a_{\xi,t}|^{2/(1+\beta)}\right). \quad (13)$$

313 where n is the dimension of \mathbf{d} . The Gaussian likelihood functions are special case of the generalized
 314 likelihood functions. For example, by setting $\beta=0$, $\xi=1$, $\phi_i=0$, $\sigma_t=\sigma_0$, $\sigma_\xi=1$, $\mu_\xi=0$,
 315 $\omega_\beta=1/\sqrt{2\pi}$, $c_\beta=1/2$, and $a_{\xi,t}=a_t$, equation (13) becomes the likelihood function corresponding
 316 to the SLS data model. Replacing $\sigma_t=\sigma_0$ by $\sigma_t=\sigma_0+\sigma_1 E_t$, equation (13) becomes the likelihood
 317 function of the WLS data model.

318 In this study, the posterior distributions of the data model parameters are jointly estimated with
 319 the soil respiration model parameters using the MT-DREAM_(ZS) code (Laloy and Vrugt, 2012).
 320 MT-DREAM_(ZS) implements a Markov chain Monte Carlo (MCMC) algorithm by running
 321 multiple Markov chains in parallel with adaptive proposal distribution, multiple-try sampling, and
 322 sampling from an archive of past states. These state-of-the-art features assist in overcoming
 323 common challenges in the sampling space such as multimodality, ill-conditioning, and high
 324 dimensionality, and thus allow for accurate exploration of the targeted distributions.

325 **2.3 Soil respiration models**

326 Zhang et al. (2014) studied the Birch effect (the peak soil microbial respiration pulses in
 327 response to episodic rainfall pulses), and developed five models, evolving from an existing four-
 328 carbon pool model to models with additional carbon pools and/or explicit representations of soil
 329 moisture controls on carbon degradation and microbial uptake rates. Three of the five models are

330 used in this study, and they are denoted as 4C, 5C, and 6C. Note that model 4C is model 4C_NOSM
 331 of Zhang et al. (2014), not their model 4C. Figure 1 is the diagram of model 6C, the most complex
 332 one among the five models. The simplest one, model 4C, has four carbon pools, i.e., soil organic
 333 carbon (SOC), dissolved organic carbon (DOC), microbial biomass (MIC), and enzymes (ENZ),
 334 and does not consider the soil moisture control on carbon degradation and microbial uptake rates.
 335 Models 5C and 6C have an explicit representation of soil moisture controls on the rates. Based on
 336 the dual Arrhenius and Michaelis–Menten kinetics model, the original SOC degradation rate,
 337 V_{decom} , is (Davidson et al., 2011; Davidson and Janssens, 2006)

$$338 \quad V_{decom} = V_{max} C_{ENZ} \frac{C_{SOC}}{K_m + C_{SOC}} \quad (14)$$

339 where V_{max} [s^{-1}] is the maximum SOC degradation rate per unit enzyme when the substrate is not
 340 limiting, C_{ENZ} [gCm^{-3}] is enzyme pool size, C_{SOC} [gCm^{-3}] is SOC pool size, and K_m is the half-
 341 saturation for SOC. The original microbial uptake rate, V_{uptake} , is (Davidson et al., 2011; Davidson
 342 and Janssens, 2006)

$$343 \quad V_{uptake} = V_{max_up} C_{MIC} \frac{C_{DOC}}{K_{m_up} + C_{DOC}} \frac{C_{O_2}}{K_{m_upO_2} + C_{O_2}}, \quad (15)$$

344 where V_{max_up} [s^{-1}] is the maximum DOC uptake rate when the substrate is not limiting, C_{MIC}
 345 [gCm^{-3}] is the MIC pool size, C_{DOC} [gCm^{-3}] is the DOC pool size, C_{O_2} [m^3m^{-3}] is the gas
 346 concentration of O_2 in the soil pore, and K_{m_up} [gCm^{-3}] and $K_{m_upO_2}$ [m^3m^{-3}] are the corresponding
 347 half-saturation constants for DOC and O_2 , respectively. With the explicit representation of soil
 348 moisture control, the two rates become (Zhang et al., 2014)

$$349 \quad V_{decom} = V_{max} C_{ENZ} \frac{C_{SOC}}{K_m + C_{SOC}} \left(\frac{\theta}{\theta_s} \right) \quad (16)$$

350
$$V_{uptake} = V_{\max_up} C_{MIC} \frac{C_{DOC}}{K_{m_up} + C_{DOC}} \frac{C_{O_2}}{K_{m_upO_2} + C_{O_2}} \left(\frac{\theta}{\theta_s} \right) \quad (17)$$

351 where θ [-] is the volumetric soil moisture, and θ_s [-] is the porosity.

352 In addition to using the new rate equations, models 5C and 6C have more carbon pools. In
 353 model 5C, DOC is split into two sub-pools for wet zone and dry zone of soil pores, and only the
 354 wet DOC is used by MIC, as shown in Figure 1. The moisture-controlled microbial uptake rate
 355 becomes

356
$$V_{uptake} = V_{\max_up} C_{MIC} \frac{C_{DOC_w}}{K_{m_up} + C_{DOC_w}} \frac{C_{O_2}}{K_{m_upO_2} + C_{O_2}} \left(\frac{\theta}{\theta_s} \right). \quad (18)$$

357 where C_{DOC_w} [gCm⁻³] is the DOC pool size in the wet soil pores. Model 6C is more complex in
 358 that ENZ is further split into two sub-pools for wet and dry pores, and both the wet and dry ENZ
 359 are subject to degradation, as shown in Figure 1. The moisture-controlled SOC degradation rate
 360 becomes

361
$$V_{decom} = V_{\max} C_{ENZ_W} \frac{C_{SOC}}{K_m + C_{SOC}} \left(\frac{\theta}{\theta_s} \right) \quad (19)$$

362 for the wet ENZ and

363
$$V_{decom} = V_{\max} C_{ENZ_D} \frac{C_{SOC}}{K_m + C_{SOC}} \left(1 - \frac{\theta}{\theta_s} \right) \varepsilon_D \quad (20)$$

364 for the dry ENZ, where C_{ENZ_W} [gCm⁻³] is the wet soil pores enzyme pool size, C_{ENZ_D} [gCm⁻³] is
 365 the enzyme pool size in the dry soil pores, and ε_D is the catalysis efficiency of the dry zone enzyme.

366 Due to considering the moisture control and adding more soil pools, model 5C is expected to
 367 be significantly better than model 4C for simulating the Birch effect. Since the accumulated ENZ
 368 in dry soil is secondary, model 6C is expected to be slightly better than model 5C. In terms of

369 model structural error, model 4C has the largest model structure error, model 5C has significantly
370 less model structure error, and model 6C has the smallest model structural error. In other words,
371 model 6C has the highest model fidelity (i.e. lowest model discrepancy) among the three models.
372 As shown below, the degree of model structural error is reflected in the process of Bayesian
373 inference and verified by the cross-validation.

374 **2.4 Observations and parameter estimation**

375 Figure 2 plots the time series of 17,016 observations of soil moisture and CO₂ efflux used in
376 this study. The observations were obtained during the entire year of 2007, covering a long period
377 of dry season prior to monsoon and episodic rainfall events during monsoon. The first two third of
378 this dataset is used for the Bayesian inference, and the last one third is used for cross-validation.
379 The inference and cross-validation periods have both dry and wet periods, as shown in Figure 2.
380 The observation site is located within the Santa Rita Experimental Range (SRER, 31.8214°N,
381 110.8661°W, elevation 1,116 m) outside of Tucson, Arizona (Barron-Gafford et al., 2011; Scott
382 et al., 2009). This savanna site was covered by 22% of perennial grass, forbs and subshrubs and
383 35% of mesquite. The soils are uniformly Comoro loamy sand (77.6% sand, 11.0% clay, and
384 11.4% silt). The half-hourly atmospheric forcing data were collected from measurements through
385 an eddy covariance tower (Scott et al., 2009). This includes downward shortwave, longwave,
386 precipitation, wind, air temperature, humidity, and pressure. Volumetric CO₂ concentration was
387 measured at a half-hourly interval through compact probes. The CO₂ efflux was estimated from
388 the gradient of CO₂ concentration measured at two depths of 2 cm and 10 cm through Fick's first
389 law of diffusion, and the estimates were validated against measurements from a portable CO₂ gas
390 analyzer.

391 The parameters estimated in this study include the parameters of the soil respiration models
 392 (4C – 6C) and the parameters of the data models described in Section 2.1. The estimated
 393 parameters of models 4C and 5C include the microbial carbon use efficiency (CUE) [g/g], enzyme
 394 production rate, k_e [g/m³s], microbial turnover rate, τ_m [1/s], and enzyme turnover rate τ_e [1/s].
 395 Uniform distributions are used as the prior in the Bayesian inference, and the ranges of the four
 396 parameters are 0.2 – 1.00, 1×10^{-12} – 1×10^{-7} , 1×10^{-12} – 1×10^{-5} and 1×10^{-11} – 1×10^{-6} , respectively.
 397 The values of other parameters are fixed at the values used in Allison et al. (2010). Model 6C has
 398 two more parameters, and they are the catalysis efficiency ε_D [-] and the turnover rate of the dry-
 399 zone enzymes τ_{en} [1/s]. The prior of the two parameters are uniform distributions with the ranges
 400 of 0.2 – 0.8 and 1×10^{-12} – 1×10^{-8} , respectively.

401 The DREAM-based MCMC simulation is conducted for a total of 24 cases, the combinations
 402 of eight data models and three soil respiration models. For each case, the parameter distributions
 403 are obtained after drawing a total of 5×10^5 samples using five Markov chains. The Gelman and
 404 Rubin (1992) R-statistic is used for convergence diagnostic, and it approaches one in less than
 405 40,000 samples. The initial 50% of the samples are discarded during the burn-in period.

406 2.5 Metrics for evaluating predictive performance

407 Three criteria are used to evaluate the predictive performance of the soil respiration models
 408 and data models, and they are central mean tendency, dispersion, and reliability. Each criterion is
 409 measured by a single metric. In addition, a newly defined metric by (Elshall et al., 2018) is also
 410 used for simultaneously measuring the three criteria.

411 The central mean tendency is measured in this study using the Nash-Sutcliffe model efficiency
 412 (NSME) coefficient (Nash and Sutcliffe, 1970),

$$413 \quad NSME = 1 - \frac{\sum_{i=1}^n (d_i - \bar{\mathbf{Y}}_i)^2}{\sum_{i=1}^n (d_i - \bar{\mathbf{d}})^2}, \quad (21)$$

414 where n is the number of cross-validation data, d_i is the i -th data, $\bar{\mathbf{d}}$ is the mean of the data, and
415 $\bar{\mathbf{Y}}_i$ is the mean of the prediction ensemble, \mathbf{Y}_i , for d_i . NSME ranges from $-\infty$ to 1, with $NSME = 1$
416 corresponding to a perfect match between data and mean prediction, i.e., the ensemble is centered
417 on the data. $NSME = 0$ indicates that the model predictions are as only accurate as the mean of the
418 data, while an efficiency $NSME < 1$ indicates that the mean of data is a better prediction than the
419 mean prediction.

420 In addition to the central mean tendency, it is also desirable that the ensemble is precise with
421 small dispersion and reliable to cover all the data. This study uses a nonparametric metric for
422 dispersion, and it is the sharpness of a prediction interval (e.g. Smith et al., 2010a)

$$423 \textit{Sharpness} = 1/n \sum_{i=1}^n [\textit{Max}(\mathbf{Y}_i) - \textit{Min}(\mathbf{Y}_i)] \quad (22)$$

424 where \mathbf{Y}_i is the prediction ensemble within the 95% prediction interval, the Bayesian credible
425 interval, not the confidence interval used in nonlinear regression (Lu et al., 2013). Smaller values
426 of sharpness indicate better prediction precision. Reliability is measured using predictive coverage.
427 (e.g. Hoeting et al., 1999), which is the percentages of data contained in the prediction interval.
428 Larger predictive coverage values are preferred.

429 To account for the trade-off between the three metrics, Elshall et al. (2018) defined relative
430 model score (RMS) that simultaneously measure all the three criteria. Scoring rules are commonly
431 used in hydrology to assess predictive performance (e.g., Weijjs et al., 2010; Westerberg et al.,
432 2011). RMS is used in this study to measure the relative predictive performance of the
433 combinations of soil respiration models and data models. For combination M_j , RMS is defined as

$$RMS(M_j) = \frac{\sum_{i=1}^n p(d_i | \mathbf{Y}_{ij}, M_j)}{\sum_{j=1}^m p(d_i | \mathbf{Y}_{ij}, M_j)} \times 100 \quad (23)$$

where m is the number of combinations; the ensemble prediction \mathbf{Y}_{ij} is similar to \mathbf{Y}_i above with index i over time and index j specific to the j -th combination. The density function $p(d_i | \mathbf{Y}_{ij})$ can be evaluated by first obtaining the density function $p(\mathbf{Y}_{ij})$ of the ensemble prediction \mathbf{Y}_{ij} (e.g., by using the kernel density function) and then evaluating $p(d_i | \mathbf{Y}_{ij})$ using interpolation methods based on the intersection of \mathbf{Y}_{ij} and d_i . More details about evaluating RMS can be found in Elshall et al. (2018). This evaluation is based purely on the model predictions, and does not involve any assumptions on the models, their parameters, and likelihood functions. Larger RMS values indicate better overall predictive performance. A figure of our workflow scheme is presented in the supplementary materials.

3 Results of Bayesian Inverse Modeling

This section analyzes the residuals of the best realization (with the highest likelihood value) of the MCMC simulation to understand whether the assumptions of the eight data models hold. The impacts of the data models on the posterior parameter distributions are also analyzed.

3.1 Residual characterization

Figure 3 shows residual plots for model 6C based on data models SLS and WSEP-AC. SLS is the simplest data model with the assumptions of homoscedastic, independent, and Gaussian residuals, and the WSEP-AC is the most complex one without the assumptions. Model 6C is the most complex model and also the best one as ranked by Zhang et al. (2014) using Bayesian model selection. The variable a_t plotted in Figures 3a-3c and Figures 3d-3f is defined in equations (2) and (11), respectively. Figures 3a – 3c show that all the three residual assumptions are violated when SLS is used, because (i) the residual variance is not constant, but increases as a function of the

456 simulated CO₂ efflux (Figure 3a); (ii) the autocorrelation function at most lags is beyond the 95%
457 confidence interval (Figure 3b); (iii) the standard normal density function cannot adequately
458 characterize the residuals (Figure 3c). Figures 3d-f show that, after relaxing the three assumptions,
459 the processed residuals, a_t , can be well characterized by WSEP-AC. Figure 3d shows that, after
460 normalizing ε_t with the linear variance ($\sigma_t = 0.034 + 0.099 E_t$), the variation of the variance of
461 a_t becomes significantly smaller, although the variance is still not constant. Figure 3e shows that,
462 after removing a first-order autoregressive model from ε_t , a_t becomes less correlated, although the
463 correlation is not fully removed. The two coefficients of the autoregressive model are $\phi_1 = 0.989$
464 and $\phi_2 = 4.5 \times 10^{-6}$; the small value of ϕ_2 indicates that there is no need to attempt an autoregressive
465 model of higher order. Figure 3f shows that a_t follows the SEP distribution with the estimated
466 skewness coefficient of $\xi = 0.933$ and kurtosis coefficient of $\beta = 0.998$. As a summary, Figure
467 3 shows that it is important to examine the residuals and to determine whether the selected data
468 model is adequate for charactering the residuals. Although WSEP-AC still cannot perfectly
469 characterize ε_t , it is significantly better than SLS.

470 Although the Gaussian assumption used in SLS is violated for model 6C (Figure 3c), this is
471 not generally the case for other data models and soil respiration models. This is shown in Figure
472 4, which presents the quantile-quantile (Q-Q) plot for the eight data models and the three soil
473 respiration models. For SLS, WLS, SLS-AC, and WLS-AC, the theoretical quantiles are based on
474 the standard normal distribution, $N(0,1)$; for SEP, WSEP, SEP-AC, and WSEP-AC, the theoretical
475 quantiles are based on the standard skew exponential power distribution, $SEP(0,1,1,0)$. If the
476 residuals follow the assumed standard distributions, the Q-Q plots fall on the 1:1 lines, marked as
477 the theoretical lines in Figure 4. If the residuals are Gaussian or SEP but not standard, the Q-Q
478 plots fall on a straight line but not the 1:1 line. Figures 4a and 4e show that, for all the soil

479 respiration models, the Q-Q plots of SLS and SEP deviate significantly from the theoretical lines
480 and exhibit fat-tail behaviors, which is an indication of outliers (Thyer et al., 2009). The deviation
481 is reduced after accounting for autocorrelation in SLS-AC and SEP-AC, as shown in Figures 4c
482 and 4g. It is interesting to observe from the two figures that the Q-Q plots of the three models are
483 almost visually identical. The deviation is almost fully removed after accounting for
484 heteroscedasticity in WLS and WSEP in that their corresponding Q-Q plots fall on the 1:1 lines,
485 especially for models 5C and 6C, as shown in Figures 4b and 4f. However, the Q-Q plots start
486 deviating from the 1:1 lines as shown in Figures 4d and 4h, after accounting for both
487 heteroscedasticity and autocorrelation in WLS-AC and WSEP-AC. As a summary, Figure 4 shows
488 that, for the numerical example of this study, either the Gaussian or the SEP distribution is valid if
489 heteroscedasticity is accounted for in the data models. However, accounting for autocorrelation in
490 the data models does not help improve the characterization of the residual distributions.

491 **3.2 Posterior parameter distributions**

492 While Figures 3 and 4 help understand validity of the three assumptions used in the data
493 models, the impacts of the data models on estimating model parameter distributions must be
494 evaluated separately. This section discusses the impact of the data model selection on parameter
495 estimation with the objective of understanding whether incorrect specification of the data model
496 necessarily leads to biased parameter estimates. Such assessment is not a trivial task for two main
497 reasons. First, microbial soil respiration models aggregate complex natural processes and spatial
498 details into simpler conceptual representations. As a results several model parameters are effective
499 values of several complex natural processes that cannot be actually measured in the field as
500 discussed by Vrugt et al. (2013). In addition, even for model parameter that can be measured in
501 the field, since the model structure is imperfect, calibrated parameter values are sometimes beyond

502 their physically reasonable range, as discussed by Pappenberger and Beven (2006). This is often
503 undesirable, if we seek to make the models more mechanistically descriptive.

504 We focus our discussion on carbon use efficiency (CUE) for microbial growth due to two
505 reasons: (1) CUE is a fundamental parameter in microbial soil respiration models, and (2) a
506 physically reasonable range for CUE can be estimated. The concept of microbial CUE (Allison et al.,
507 2010; Bradford et al., 2008; Manzoni et al., 2012; Wieder et al., 2013) has been used to present
508 fundamental microbial processes in recent microbial enzyme models (Allison et al., 2010; German
509 et al., 2011; Schimel and Weintraub, 2003; Wang et al., 2013). The microbial CUE, which is
510 marked between MIC and CO₂ in Figure 1, controls microbial growth, enzyme production and
511 microbial respiration. A physically reasonable range of CUE can be estimated from the physical
512 viewpoint (Tang and Riley, 2014). Sinsabaugh et al. (2013) showed that the thermodynamic
513 calculations support a maximum CUE of 0.60 and that previous studies that estimate CUE in
514 terrestrial systems report a mean value of 0.55. Theoretically, there is no lower limit for CUE as it
515 can approach zero, and $CUE < 0.1$ has been reported for terrestrial ecosystems (e.g., Fernández-
516 Martínez et al., 2014) and used in modeling studies (Li et al., 2014). Note that, for inverse modeling
517 with MCMC sampling, we did not assume CUE maximum value of 0.6. In other words, for
518 parameter estimation and predictive performance we did not impose the constraint that CUE is less
519 than 0.6. We merely use this CUE maximum value of 0.6 to evaluate whether the posterior CUE
520 parameter samples obtained using different data models and different soil respiration models are
521 within the physically reasonable range of $0 \sim 0.6$.

522 Figure 5 plots the CUE posterior marginal density of the three soil respiration models obtained
523 using the eight data models. The physical range between zero and 0.6 is marked in yellow. Figure
524 5 shows that the CUE posterior parameter distribution of Model 6C obtained using the data models

525 that does not account for autocorrelation are within the physically reasonable range. For models
526 4C and 5C, the posterior parameter samples are outside the range for six data models. For model
527 4C, the posterior parameters are within the physical range only for data models SEP and WSEP;
528 for model 5C, the two data models are WLS and WSEP. It is not surprising to find the posterior
529 parameter distribution of models 4C and 5C, which have a certain degree of model structure error,
530 to be out of the physically plausible range. This can be attributed to two reasons. First, the model
531 solution can be biased toward the missing processes in the model structure such as the additional
532 carbon pool in both 4C and 5C or missing the explicit accounting for soil moisture in 4C. Second,
533 biased parameter estimation can compensate for model structure inadequacy and other sources of
534 discrepancy in both the physical models and the data models.

535 In addition, it is important to understand how accounting for autocorrelation, heteroscedasticity
536 and non-Gaussian residuals can affect the parameter estimation. First, it is observed in Figure 5e-
537 h that biased parameter estimates are outside the physically reasonable range when autocorrelation
538 is explicitly accounted for. This may suggest again that accounting for heteroscedasticity is
539 desirable but accounting for autocorrelation is not. A possible reason is that filtering
540 autocorrelation may reduce the residual space such that the transformed residual space cannot
541 correspond to the parameter space of the models. In other words, parameter information may be
542 lost due to filtering out autocorrelation. However, it is not fully understood why this does not occur
543 for the model 6C under data model SLS-AC (Figure 5e), and more research is warranted. Second,
544 unlike accounting for auto-correlation, accounting only for heteroscedasticity (i.e., WLS and
545 WSEP) only amplifies or reduces the variance without affecting the structure of the residual space.
546 Figures 5c-d show that account for heteroscedasticity (i.e. WLS and WSEP) tends to improve the
547 parameter estimation in comparison with homoscedastic data models (i.e., SLS and SEP) shown

548 in Figure 5a-b. Finally, with respect to non-Gaussian residuals, Schoups and Vrugt (2010)
549 suggested that, compared to Gaussian pdf, the peaked pdf of the SEP with a longer tail is useful
550 for making parameter inference robust against outliers. To a certain degree, this can be
551 substantiated by the results in Figure 5a-d, in that SEP and WSEP provide more favorable
552 parameter estimates than SLS and WLS.

553 Finally, Figure 5a shows that the posterior parameter distributions of SLS are very narrow for
554 the three soil respiration models. The narrow distributions can be attributed to several reasons.
555 Since SEP distribution can have longer tails than Gaussian distribution, this can further increase
556 the samples acceptance ratio from tails resulting in wider distribution (Figure 5b). In addition,
557 accounting for heteroscedasticity will result in wider posterior parameter distribution (Figure 5c)
558 due to accepting higher variances at peak effluxes. Moreover, filtering correlation (Figure 5e-h)
559 increases the entropy, and leads to wider distributions.

560 **4. Results of Predictive Performance**

561 Based on the last one third of the CO₂ efflux observations, a cross-validation test was
562 conducted for the combinations of three soil respiration models and eight data models. For the
563 cross-validation period, the predictive performance is examined using the four statistical metrics
564 that are defined in Section 2.5. The metrics are also calculated for the calibration period. This is
565 not to perform Bayesian model selection given the calibration data, but to better understand the
566 impact of data models on predictive performance of the three soil respiration models. For each
567 calibration and each cross-validation data, a prediction ensemble is generated from the two
568 perspectives of parametric uncertainty only and total uncertainty, as presented in Section 4.1 and
569 4.2, respectively.

570

571 **4.1 Predictive performance with parametric uncertainty of soil respiration model**

572 In this section the ensemble is generated by running the soil respiration models with the
573 posterior samples (obtained from the Bayesian inference) of the physical model parameters. In
574 other words, the ensemble addresses parametric uncertainty of the soil respiration models only.
575 Considering the relative contribution of parametric uncertainty only will provide insights for
576 modeling approaches that attempt to segregate various sources of uncertainty (e.g., Thyer et al.,
577 2009 ; Tsai and Elshall, 2013). The four statistics above (i.e. NSME, sharpness, coverage, and
578 RMS) are calculated for the three soil respiration models and the eight data models. Taking data
579 models SLS and WSEP-AC as an example, Figure 6 plots the data (for the calibration and cross-
580 validation periods separately) along with the mean and 95% credible intervals of the prediction
581 ensemble for the three models.

582 Figure 6 shows that the data models affect model simulations for all the models. The statistics,
583 especially RMS, indicate that WSEP-AC has better predictive performance than SLS. This is most
584 visually obvious for model 6C during the cross-validation period after 330 days, as the prediction
585 ensemble of SLS (Figure 6k) cannot cover the observations, whereas the prediction ensemble of
586 WSEP-AC can (Figure 6l). This conclusion that WSEP-AC outperforms SLS agrees with that
587 drawn from Figures 3 and 4.

588 Figure 7 plots the four statistics for all the soil respiration models and data models. Figures 7a
589 and 7b show the predictive performance with respect to the central mean tendency measured by
590 NSME for both the calibration and cross-validation periods respectively. The results indicate that,
591 under all data models, the low fidelity model 4C over-fits the data and results in biased predictions,
592 in that the NSME values become significantly worse (e.g., from 0.6 to -0.6) from the calibration
593 to the cross-validation period. This is confirmed by the visual inspection of Figures 6a and 6g for

594 data model SLS and of Figures 6b and 6h for data model WSEP-AC. For models 5C and 6C, their
595 NSME values vary with the data models; and the central mean accuracy is the worst for SLS-AC
596 that considers only autocorrelation (Figure 6b).

597 With respect to parametric uncertainty estimation, Figures 7c and 7d show that sharpness
598 generally increases when the three assumptions in the data models are gradually relaxed from SLS
599 to WSEP-AC. This is even more obvious during the validation period. Given that the prediction
600 ensemble does not center on the data, the increasing sharpness is desirable as it improves
601 reliability. This is confirmed by the reliability plots in Figures 7e and 7f. The exceptions are again
602 for SLS-AC and SEP-AC that generally have the lowest coverage.

603 With respect to the overall predictive performance measured by RMS, the same variation
604 pattern and exception are also observed in the RMS plots in Figures 7g and 7h. This is not
605 surprising because RMS is the metric that can be used to measure all the three criteria (central
606 mean tendency, sharpness, and reliability). Since the prediction ensemble is not centered on the
607 data, the sharpness and reliability are the decisive factors for evaluating the predictive
608 performance.

609 As a summary, while it is necessary to account for heteroscedasticity in a data model, caution
610 is needed when accounting for autocorrelation in the manner described in Section 2.1. In addition,
611 after comparing the RMS values of the residuals using the Gaussian and SEP distributions, the
612 conclusion is that the SEP distribution outperforms the Gaussian distribution with respect to
613 predictive performance. Finally, uncertainty underestimation is evidenced by the very small
614 predictive coverage. The underestimation of uncertainty for all the physical models with all the
615 data model is not unexpected because only parametric uncertainty is considered in this study.
616 Considering the overall predictive uncertainty is the subject of the next section.

617 4.2 Predictive performance with total uncertainty

618 The simulated output $\mathbf{Y}(\boldsymbol{\theta}_p)$ is generally not equal to the observed output \mathbf{d} , and we have a
619 residual term $\boldsymbol{\varepsilon}$ due to measurement, input and model structure errors such that $\mathbf{d} = \mathbf{Y}(\boldsymbol{\theta}_p) + \boldsymbol{\varepsilon}$.
620 Accounting for the error term $\boldsymbol{\varepsilon}$ can be through separating various error terms. For example, in
621 section 4.1 we obtained uncertainty due to the physical model parameters. Accounting for other
622 sources of uncertainty can be done using a single model approach (e.g. Thyer et al., 2009) or a
623 multi-model approach (e.g. Tsai and Elshall, 2013). Alternatively, we can quantify the uncertainty
624 based on total residuals that separates out parametric uncertainty, so the residual error includes
625 errors in measurements, model inputs, and model structures (e.g. Thyer et al., 2009; Schoups and
626 Vrugt, 2010). This lumped approach is based on sampling the residuals model $\boldsymbol{\varepsilon}(\boldsymbol{\theta}_\varepsilon)$ with
627 parameters $\boldsymbol{\theta}_\varepsilon$. SLS has one fixed parameter that is the constant variance, and other data models
628 have two to six parameters. Thus in this section the prediction ensemble addresses parametric
629 uncertainty of not only the soil respiration models but also the data models. When generating the
630 prediction ensemble in the procedure described by Schoups and Vrugt (2010), an ensemble of
631 residuals is first generated by running the data models with posterior samples of the data model
632 parameters for the positive carbon efflux domain; the residual ensemble is then added to the
633 prediction ensemble generated in Section 4.1.

634 We start by a visual assessment of the predictive performance. Figure 8 is similar to Figure 6
635 with the exception that Figure 8 considers the overall predictive uncertainty (i.e. parametric and
636 output uncertainty), while Figure 6 considers the parametric uncertainty only. Figure 8 reveals a
637 practical observation about accounting for the overall uncertainty through the lumped approach of
638 sampling the data models. For example, Figure 8b shows that, despite the wide prediction interval
639 of model 4C, the model with significant model structure error cannot capture the birch pulse around

640 day 180. It indicates that proper using a data model for model residuals cannot compensate
641 significant model structure error.

642 Figure 9 plots the four statistics (NSME, sharpness, predictive coverage, and RMS) of the three
643 soil respiration models under the eight data models to assess the predictive performance. With
644 respect to central mean tendency, the NSME values in Figures 9a-9b are visually the same as those
645 in Figures 7a-7b, indicating that the central mean accuracy under parametric uncertainty is the
646 same as that under predictive uncertainty.

647 With respect to uncertainty, the values of sharpness and predictive coverage increase
648 substantially (Figures 9c – 9f). In particular, Figures 9e and 9f show that, except for SLS and SEP,
649 the predictive coverage of the rest of the six data models are close to 100% for all the three soil
650 respiration models, indicating that the prediction intervals cover almost all the data. This is
651 demonstrated in Figures 6 for WSEP-AC. Similar to Figures 7c and 7d, Figures 9c and 9d also
652 show a general pattern that the sharpness increases when the three assumptions in the data models
653 are gradually relaxed from SLS to WSEP-AC. The data models that account for autocorrelation
654 are still the exceptions.

655 With respect to the overall predictive performance, the RMS values are largely determined by
656 the mean accuracy and sharpness as the predictive coverage is similar for different data models.
657 Figures 9g and 9h of RMS show that the predictive performance of the four data models that
658 account for autocorrelation is worse than that of the other four data models. This suggests again
659 that one needs to be cautious when building autocorrelation into a data model. This is consistent
660 with the finding of Evin et al. (2013, 2014) that accounting for autocorrelation before accounting
661 for heteroscedasticity or jointly accounting for autocorrelation and heteroscedasticity can result in
662 poor predictive performance. In summary, Figures 9g and 9h show for both the calibration and

663 prediction periods that accounting for heteroscedasticity in WLS and WSEP gives the best overall
664 predictive performance, and accounting for autocorrelation without heteroscedasticity in SLS-AC
665 and SEP-AC gives the worst overall predictive performance. Finally, for the three soil respiration
666 models, RMS shows that model 4C has the worst predictive performance for both the calibration
667 and cross-validation data. Generally speaking, the high fidelity model 6C outperforms model 5C
668 for both the calibration and cross-validation data, which justifies the complexity of model 6C.

669 To demonstrate the impacts of the data models on predictive performance of the soil respiration
670 models, Figure 10 plots the model simulations and predictions given by model 6C during the
671 calibration and cross-validation periods using all the eight data models. Figure 10 is used to
672 investigate predictive performance characteristics of the different data models. By examining the
673 predictive performance of model 6C, specific predictive performance patterns can be identified.
674 Figures 10a – 10d show that SLS and SEP have similar predictive performance with SEP generally
675 having better predictive performance especially during the validation period. Not accounting for
676 heteroscedasticity will underestimate the predication uncertainty (Figure 10b and Figure 10d). This
677 is mainly because the variance of the efflux residuals increases with the magnitude of the carbon
678 effluxes (Figure 3a), and thus assuming constant variance is not representative. Accordingly,
679 accounting for heteroscedasticity using WLS (Figure 10e) or WSEP (Figure 10h) will make the
680 predictions more sensitive to peck carbon effluxes. This will generally improve the predictive
681 coverage on the expense of sharpness and the central mean tendency. While WLS and WSEP have
682 similar predictive performance, WSEP has better central mean tendency and overall predictive
683 performance than WLS. Figures 10i – 10l show that accounting for autocorrelation using SLS-AC
684 and SEP-AC results in wider uncertainty bands and insensitivity to peak carbon effluxes as
685 compared to SLS and SEP (Figures 10a-d), which may be due to reduction of information content

686 of the residuals. This results in deteriorating the sharpness, the central mean tendency and the
687 capturing of peak carbon fluxes, especially during the validation period. Figures 10m – 10p show
688 that accounting for both heteroscedasticity and autocorrelation using WLS-AC and WSEP-AC
689 makes the inference robust against peak carbon effluxes. However, due to the loss of information
690 content, the uncertainty bands are still wider, and uncertainty becomes overestimated especially
691 during validation period as compared to WLS and WSEP (Figures 10e – 10h). The results of
692 Models 4C and 5C, which are not shown here, also show the same prediction patterns with respect
693 to non-Gaussian residuals, heteroscedasticity, and autocorrelation.

694 Finally, we observe in Figure 10 that the data models that have good overall predictive
695 performance as measured by RMS during the calibration period will maintain this good predictive
696 performance during the validation period. For model 6C, RMS values for the calibration and
697 validation periods are very well correlated with a correlation coefficient of 0.92. However, we note
698 that for models 4C and 5C the overall predictive performances during the calibration and validation
699 periods are not that well correlated as 6C, with correlation coefficients of 0.52 for model 4C and
700 0.61 for model 5C. This suggests that model 6C is more robust than 4C and 5C for forecasting and
701 hindcasting.

702 **4.3 Discussion on handling residual correlation**

703 Accounting for autocorrelation can lead to biased parameter estimation (Figure 5) and poor
704 predictive performance (Figure 10). Auto-correlated residuals may be attributed to model
705 discrepancy, as shown in Lu et al. (2013). The most obvious solution to handle the autocorrelation
706 is to reduce the autocorrelation by improving the soil respiration model. If model improvement is
707 difficult for practical reasons, we can improve the data model to better characterize the

708 autocorrelation. Addressing autocorrelation in a data model is challenging since it involves several
709 interlinked factors as follows:

710 (1) Non-stationarity due to wet-dry periods could be a reason for this problem. By drawing on
711 similarity from surface hydrology, the study of Ammann et al. (2018) suggests that auto-
712 correlated residuals might be attributed to non-stationarity due to wet-dry periods with half-
713 hourly data. Accounting for non-stationarity could better address the problem of auto-
714 correlated residuals (Ammann et al., 2018; Smith et al., 2010b).

715 (2) The way of implementing autocorrelation could have an impact. Autocorrelation could be
716 applied to raw residuals directly (e.g., Li et al., 2015), to transformed residuals based on
717 covariance matrix of residuals $L(\mathbf{e})$ (e.g., Lu et al., 2013), or to normalized residuals $L(\mathbf{a})$ (e.g.,
718 Schoups and Vrugt, 2010; Evin et al., 2013). Note that \mathbf{e} is a vector of transformed residuals,
719 while \mathbf{a} denotes a vector of independent and identically distributed random errors with zero
720 mean and unit standard deviation. The $L(\mathbf{e})$ approach based on covariance matrix of residuals
721 is generally limited to Gaussian data models (e.g. Lu et al., 2013), while the $L(\mathbf{a})$ approach for
722 normalized residuals can be readily adopted for non-Gaussian data models.

723 (3) The autocorrelation model could have an impact. Using an autoregressive model is a popular
724 technique to account for auto-correlated residuals. However, using an autoregressive model
725 with either joint inversion approach (e.g., this study and Schoups and Vrugt, 2010) or
726 sequential approaches (e.g., Evin et al., 2013, 2014; Lu et al., 2013) removes correlation errors
727 through a filter approach, which can lead to a loss of information content. As this may cause
728 overcorrection of prediction especially at surge events, Li et al. (2015) developed a restricted
729 autoregressive model to overcome this adverse effect. Other autocorrelation models include
730 moving average model and mixed autoregressive-moving averaging model (Chatfield, 2004).

731 (4) Joint versus sequential inversion for autocorrelation could have an impact. Sequential inversion
732 approaches include two-step procedures (e.g. Evin et al., 2013, 2014; Lu et al., 2013) or the
733 multi-step procedure (Li et al., 2016a). These sequential approach estimates the autoregressive
734 parameters sequentially in a later step after estimating the physical model parameters and other
735 data model parameters. Evin et al. (2013, 2014) used a sequential approach to avoid the
736 interaction between the parameters of the heteroscedasticity model and the autocorrelation
737 model. In addition, the autoregressive model parameters can be deterministically calculated as
738 an internal variables of the data model similar to Lu et al. (2013), and not as calibration
739 parameters (e.g. Schoups and Vrugt; Evin et al. 2013; 2014). While the first step in the
740 sequential approach would avoid the biased parameter estimation (Figure 10a-d), the second
741 step can still lead a poor predicative performance since we are essentially using a filter
742 approach to remove residual correlation. To address this problem, Li et al. (2016) multi-step
743 procedure that is based on Gaussian data model uses restricted autoregressive model.
744 Generally, Ammann et al. (2018) states that the joint inversion is still preferred, and
745 understanding the conditions where accounting for auto-correlation can be achieved remain
746 poorly understood.

747 **5. Conclusions**

748 In parameter estimation and prediction of soil carbon fluxes to the atmosphere, one often
749 assumes that residuals, which include errors in observations, model inputs, parameter estimates,
750 and model structures, are normally distributed, homoscedastic and uncorrelated. We study these
751 assumptions by calibrating three soil inspiration models, which have varying degrees of model
752 structure errors. We further explore eight data models that characterize the residuals statistically
753 by starting with the standard least squares (SLS) and skew exponential power (SEP) data models

754 that assume homoscedastic and non-correlated residuals. For these two distributions, we evaluate
755 six other data models that account for heteroscedasticity (WLS and WSEP), autocorrelation (SLS-
756 AC and SEP-AC), and joint inversion of heteroscedasticity and autocorrelation (WLS-AC and
757 WSEP-AC). To our knowledge this is the first study that provides such detailed analysis for soil
758 reparation inverse modeling. We also use three soil respiration models with different degrees of
759 model fidelity (i.e., model discrepancy) and model complexity (i.e. number of model parameters)
760 to understand the impact of model discrepancy on the calibration results under different data
761 models. We analyze the results with respect to (1) residual characterization, (2) parameter
762 estimation, (3) predictive performance, and (4) impacts of model discrepancy. The main findings
763 of this study are summarized as follows:

764 (1) With respect to residual characterization, residual analysis results suggest that the common
765 assumption of not accounting for heteroscedasticity and residual autocorrelation in the data
766 models SLS and SEP results in poor characterization of residuals. Explicit accounting for
767 heteroscedasticity in WLS and WSEP results in significantly improved characterization of the
768 residuals, and the improvement is larger than that obtained by accounting for both
769 heteroscedasticity and autocorrelation in WSL-AC and WSEP-AC. Accounting for
770 autocorrelation only in SLS-AC and SEP-AC does not significantly improve the
771 characterization of the residuals.

772 (2) With respect to parameter estimation, the impacts of the data models are evaluated by focusing
773 on carbon use efficiency (CUE), which is a central parameter in soil respiration modeling.
774 Using SLS yields relatively reasonable posterior parameter distributions for CUE , yet very
775 narrow posterior. The data models SLS-AC, SEP-AC, WLS-AC and WSEP-AC that consider
776 autocorrelation tend to yield CUE estimates that are physically unreasonable. We speculate

777 that filtering residual correlation can affect the mapping of the model physics (as implicitly
778 included in the residuals) into the parameter space, which might result in biased parameter
779 estimates that are physically unreasonable.

780 (3) With respect to predictive performance, it is measured by four statistical criteria: central mean
781 tendency, sharpness, coverage, and relative model score for both the calibration and the cross-
782 validation periods. Results show that accounting for autocorrelation in SLS-AC, SEP-AC,
783 WLS-AC, and WSEP-AC deteriorates the predictive performance, such that the predictive
784 performance is inferior to that of SLS in terms of the central mean tendency and overall
785 predictive performance (measured by the relative model score), especially during the cross-
786 validation period. Results also indicates that using the SEP distribution can potentially improve
787 the predictive performance. The same is true for accounting for heteroscedasticity. Using SEP
788 distribution and accounting for heteroscedasticity (i.e. WSEP) can potentially improve the
789 predictive performance.

790 (4) With respect to the impact of model discrepancy, the high fidelity model (6C) gives the best
791 results with respect to parameter estimation and predictive performance. Model 6C generally
792 maintains its superior performance under different data models. This justifies the complexity
793 of model 6C relative to model 5C that has one less carbon pool. Model 4C with the lowest
794 fidelity maintains its poor performance for different data models, because the model has only
795 four carbon pools and lacks the explicit representation of soil moisture control.

796 Based on the empirical findings above, we conclude the following:

797 (1) Not accounting for heteroscedasticity and autocorrelation using a Gaussian or non-Gaussian
798 data model might not necessarily result in biased parameter estimates or biased predictions

799 with respect to central mean tendency, but will definitely underestimate uncertainty resulting
800 in lower overall predictive performance.

801 (2) Using a non-Gaussian data model can improve parameter estimation and predictive
802 performance with respect to central mean tendency and uncertainty quantification.

803 (3) Accounting for heteroscedasticity improves the uncertainty estimation with respect to
804 reliability at the cost of having a wider predictive interval.

805 (4) This study confirms other empirical findings and theoretical analyses (Evin et al., 2013; 2014;
806 Li et al., 2015, Ammann et al. 2018) that separately accounting for autocorrelation or jointly
807 accounting for autocorrelation and heteroscedasticity can be problematic. While the reasons
808 remain poorly understood (Ammann et al., 2018), it might be attributed to non-stationarity due
809 to wet-dry periods with half-hourly data (Ammann et al., 2018) or to the method of handling
810 autocorrelation (e.g., Schoups and Vrugt, 2010, Evin et al., 2013; 2014; Lu et al., 2013; Li et
811 al., 2015, 2016a; Ammann et al. 2018). Further investigation to address autocorrelation in soil
812 respiration modeling is warranted in a future study.

813 The above conclusions are subject to several limitations. First, the conclusions are specific to
814 the soil respiration models developed and validated for semi-arid savannah. Performance
815 variations across different soil respiration models with different levels of complexities is possible.
816 Second, the conclusions are conditioned on the data that were obtained at the half-hour interval
817 over a one-year period. Different conclusions are possible if the data are thinned to daily or weekly
818 scales or data of longer observation periods are used. Third, our study investigates effects of the
819 residual assumptions of formal likelihood functions through direct conditioning of the residuals
820 model parameters, yet this can also be done through other approaches such as residuals
821 transformation (Thiemann et al., 2001), autogressive bias model (Del Giudice et al., 2013),

822 approximate Bayesian computation (Sadegh and Vrugt, 2013), and data assimilation (Spaaks and
823 Bouten, 2013). Comparing different methods for accounting the residual assumptions are beyond
824 the scope of this work. Fourth, this study focuses on formal Bayesian computation using formal
825 likelihood functions, and comparison with other inference functions such as informal likelihood
826 functions or approximate Bayesian computation is warranted in a future study.

827 Based on the aforesaid conclusions and limitations, we recommend to start calibrating soil
828 respiration models with simple SLS or SEP likelihood function. If the residuals characterization is
829 adequate (e.g., Scharnagl et al., 2011), then the underlying assumptions are met. Otherwise,
830 increase complexity of the data model until satisfactory results are obtained in terms of residuals
831 characterization, posterior parameter estimation, and predictive performance. This is similar to the
832 procedure given in Smith et al. (2015). Although the empirical findings of this study provide
833 general guidelines for data model selection for soil respiration modeling, more comparative studies
834 are needed to validate and refute the findings of this study.

835 **Acronyms**

836	4C	Four carbon pool model
837	5C	Five carbon pool model
838	6C	Six carbon pool model
839	CUE	Microbial carbon use efficiency
840	DOC	Dissolved organic carbon
841	ENZ	Enzymes
842	MCMC	Markov chain Monte Carlo
843	MIC	Microbial biomass
844	NSME	Nash-Sutcliffe model efficiency
845	PDF	Probability density function
846	RMS	Relative model score
847	SEP	Skew exponential power distribution
848	SEP-AC	Skew exponential power distribution with autocorrelation
849	SLS	Standard least square
850	SLS-AC	Standard least square with autocorrelation
851	SOC	Soil organic carbon
852	WLS	Weighted least squared
853	WLS-AC	Weight least square with autocorrelation

854 WSEP Weighted skew exponential power distribution
855 WSEP-AC Weighted skew exponential power distribution with autocorrelation

856

857 **Code and data availability**

858 The data and codes and models used to produce this paper are available on contact of the
859 corresponding author at mye@fsu.edu. We cannot publicly share the workflow because MT-
860 DREAM_(ZS) code (Laloy and Vrugt, 2012) , which is a main component in the workflow, is in the
861 process of becoming a commercial code.

862 **Author contributions**

863 ASE developed and implemented the code for the eight data models for soil respiration modeling,
864 and prepared the manuscript with contribution of all co-authors. MY developed the research idea
865 and outline, and supervised the research implementation when ASE was a post-doc at Florida State
866 University. GN developed the soil respiration models. GAB collected and processed the eddy-
867 covariance data used for model calibration.

868 **Competing interests**

869 The authors declare that they have no conflict of interest.

870 **Acknowledgement**

871 The first two authors were supported by the U.S. Department of Energy grant DE-SC0008272.
872 The first author was also partly supported by the U.S. National Science Foundation Award# OIA-
873 1557349. The second author was also partly supported by U.S. Department of Energy grant DE-
874 SC0019438 and U.S. National Science Foundation grant EAR-1552329. We thank two anonymous
875 reviewers for providing comments that helped to improve the manuscript.

876 **References**

877 Ahrens, B., Reichstein, M., Borken, W., Muhr, J., Trumbore, S. E. and Wutzler, T.: Bayesian
878 calibration of a soil organic carbon model using ΔC measurements of soil organic carbon

879 and heterotrophic respiration as joint constraints, *Biogeosciences*, 11(8), 2147–2168,
880 doi:10.5194/bg-11-2147-2014, 2014.

881 Allison, S. D., Wallenstein, M. D. and Bradford, M. A.: Soil-carbon response to warming
882 dependent on microbial physiology, *Nat. Geosci.*, 3, 336 [online] Available from:
883 <http://dx.doi.org/10.1038/ngeo846>, 2010.

884 Ammann, L., Reichert, P. and Fenicia, F.: A framework for likelihood functions of deterministic
885 hydrological models, *Hydrol. Earth Syst. Sci.*, (August), 2018.

886 Bagnara, M., Sottocornola, M., Cescatti, A., Minerbi, S., Montagnani, L., Gianelle, D. and
887 Magnani, F.: Bayesian optimization of a light use efficiency model for the estimation of
888 daily gross primary productivity in a range of Italian forest ecosystems, *Ecol. Modell.*, 306,
889 57–66, doi:10.1016/j.ecolmodel.2014.09.021, 2015.

890 Bagnara, M., Oijen, M. Van, Cameron, D., Gianelle, D., Magnani, F. and Sottocornola, M.:
891 Bayesian calibration of simple forest models with multiplicative mathematical structure :
892 A case study with two Light Use Efficiency models in an alpine forest, *Ecol. Modell.*,
893 371(January), 90–100, doi:10.1016/j.ecolmodel.2018.01.014, 2018.

894 Barr, J. G., Engel, V., Fuentes, J. D., Fuller, D. O. and Kwon, H.: Modeling light use efficiency in
895 a subtropical mangrove forest equipped with CO₂ eddy covariance, *Biogeosciences*, 10(3),
896 2145–2158, doi:10.5194/bg-10-2145-2013, 2013.

897 Barron-gafford, G. A., Cable, J. M., Bentley, L. P., Scott, R. L., Huxman, T. E., Jenerette, G. D.
898 and Ogle, K.: Quantifying the timescales over which exogenous and endogenous
899 conditions affect soil respiration, *New Phytol.*, 2014.

900 Barron-Gafford, G. A., Scott, R. L., Jenerette, G. D. and Huxman, T. E.: The relative controls of
901 temperature, soil moisture, and plant functional group on soil CO₂ efflux at

902 diel, seasonal, and annual scales, *J. Geophys. Res. Biogeosciences*, 116(1), 1–16,
903 doi:10.1029/2010JG001442, 2011.

904 Berryman, E. M., Frank, J. M., Massman, W. J. and Ryan, M. G.: Agricultural and Forest
905 Meteorology Using a Bayesian framework to account for advection in seven years of
906 snowpack CO₂ fluxes in a mortality-impacted subalpine forest, *Agric. For. Meteorol.*,
907 249(April 2017), 420–433, doi:10.1016/j.agrformet.2017.11.004, 2018.

908 Box, G. E. P. and Tiao, G. C.: *Bayesian inference in statistical analysis*, Wiley., 1992.

909 Braakhekke, M. C., Beer, C., Schrumpf, M., Ekici, A., Ahrens, B., Hoosbeek, M. R., Kruijt, B.,
910 Kabat, P. and Reichstein, M.: The use of radiocarbon to constrain current and future soil
911 organic matter turnover and transport in a temperate forest, *J. Geophys. Res.*
912 *Biogeosciences*, 372–391, doi:10.1002/2013JG002420.Received, 2014.

913 Bradford, M. A., Davies, C. A., Frey, S. D., Maddox, T. R., Melillo, J. M., Mohan, J. E., Reynolds,
914 J. F., Treseder, K. K. and Wallenstein, M. D.: Thermal adaptation of soil microbial
915 respiration to elevated temperature, *Ecol. Lett.*, 11(12), 1316–1327, doi:10.1111/j.1461-
916 0248.2008.01251.x, 2008.

917 Braswell, B. H., Sacks, W. J., Linder, E. and Schimel, D. S.: Estimating diurnal to annual
918 ecosystem parameters by synthesis of a carbon flux model with eddy covariance net
919 ecosystem exchange observations, *Glob. Chang. Biol.*, 335–355, doi:10.1111/j.1365-
920 2486.2005.00897.x, 2015.

921 Cable, J. M., Ogle, K., Williams, D. G., Weltzin, J. F. and Huxman, T. E.: Soil Texture Drives
922 Responses of Soil Respiration to Precipitation Pulses in the Sonoran Desert : Implications
923 for Climate Change, *Ecosystems*, 961–979, doi:10.1007/s10021-008-9172-x, 2008.

924 Cable, J. M., Ogle, K., Lucas, R. W., Huxman, T. E., Loik, M. E., Smith, S. D., Tissue, D. T.,

925 Ewers, B. E., Pendall, E., Welker, J. M., Charlet, T. N., Cleary, M., Griffith, A., Nowak,
926 R. S., Rogers, M., Steltzer, H., Sullivan, P. F. and Gestel, N. C. Van: The temperature
927 responses of soil respiration in deserts : a seven desert synthesis, *Biogeochemistry*, 71–90,
928 doi:10.1007/s10533-010-9448-z, 2011.

929 Chatfield, C.: *The analysis of time series : an introduction*, Chapman & Hall/CRC. [online]
930 Available from: [https://www.crcpress.com/The-Analysis-of-Time-Series-An-](https://www.crcpress.com/The-Analysis-of-Time-Series-An-Introduction-Sixth-Edition/Chatfield/p/book/9781584883173)
931 [Introduction-Sixth-Edition/Chatfield/p/book/9781584883173](https://www.crcpress.com/The-Analysis-of-Time-Series-An-Introduction-Sixth-Edition/Chatfield/p/book/9781584883173) (Accessed 9 April 2019),
932 2004.

933 Chevallier, F. and O’Dell, C. W.: Error statistics of Bayesian CO₂ flux inversion schemes as seen
934 from GOSAT, *Geophys. Res. Lett.*, 40(6), 1252–1256, doi:10.1002/grl.50228, 2013.

935 Correia, A. C., Minunno, F., Caldeira, M. C., Banza, J., Mateus, J., Carneiro, M., Wingate, L.,
936 Shvaleva, A., Ramos, A., Jongen, M., Bugalho, M. N., Nogueira, C., Lecomte, X. and
937 Pereira, J. S.: Agriculture , Ecosystems and Environment Soil water availability strongly
938 modulates soil CO₂ efflux in different Mediterranean ecosystems : Model calibration
939 using the Bayesian approach, *Agric. Ecosyst. Environ.*, 161, 88–100,
940 doi:10.1016/j.agee.2012.07.025, 2012.

941 Davidson, E. A. and Janssens, I. A.: Temperature sensitivity of soil carbon decomposition and
942 feedbacks to climate change, *Nature*, 440, 165 [online] Available from:
943 <http://dx.doi.org/10.1038/nature04514>, 2006.

944 Davidson, E. A., Samanta, S., Caramori, S. S. and Savage, K.: The Dual Arrhenius and Michaelis–
945 Menten kinetics model for decomposition of soil organic matter at hourly to seasonal time
946 scales, *Glob. Chang. Biol.*, 18(1), 371–384, doi:10.1111/j.1365-2486.2011.02546.x, 2011.

947 Du, Z., Nie, Y., He, Y., Yu, G. and Wang, H.: *Tellus B : Chemical and Physical Meteorology*

948 Complementarity of flux- and biometric-based data to constrain parameters in a terrestrial
949 carbon model Complementarity of flux- and biometric-based data to constrain parameters
950 in a terrestrial carbon model, *Tellus B Chem. Phys. Meteorol.*, 0889,
951 doi:10.3402/tellusb.v67.24102, 2015.

952 Du, Z., Zhou, X., Shao, J., Yu, G., Wang, H., Zhai, D., Xai, J. and Luo, Y.: *Journal of Advances*
953 *in Modeling Earth Systems, J. Adv. Model. Earth Syst.*, 548–565,
954 doi:10.1002/2016MS000687.Received, 2017.

955 Elshall, A. S. and Tsai, F. T.-C.: Constructive epistemic modeling of groundwater flow with
956 geological structure and boundary condition uncertainty under the Bayesian paradigm, *J.*
957 *Hydrol.*, 517, doi:10.1016/j.jhydrol.2014.05.027, 2014.

958 Elshall, A. S., Ye, M., Pei, Y., Zhang, F., Niu, G.-Y. and Barron-Gafford, G. A.: Relative model
959 score: a scoring rule for evaluating ensemble simulations with application to microbial soil
960 respiration modeling, *Stoch. Environ. Res. Risk Assess.*, doi:10.1007/s00477-018-1592-3,
961 2018a.

962 Elshall, A. S., Ye, M., Pei, Y., Zhang, F., Niu, G.-Y. and Barron-Gafford, G. A.: Relative model
963 score: a scoring rule for evaluating ensemble simulations with application to microbial soil
964 respiration modeling, *Stoch. Environ. Res. Risk Assess.*, 32(10), 2809–2819,
965 doi:10.1007/s00477-018-1592-3, 2018b.

966 Evin, G., Kavetski, D., Thyer, M. and Kuczera, G.: Pitfalls and improvements in the joint inference
967 of heteroscedasticity and autocorrelation in hydrological model calibration, *Water Resour.*
968 *Res.*, 49(7), 4518–4524, doi:10.1002/wrcr.20284, 2013.

969 Evin, G., Thyer, M., Kavetski, D., McInerney, D. and Kuczera, G.: Comparison of joint versus
970 postprocessor approaches for hydrological uncertainty estimation accounting for error

971 autocorrelation and heteroscedasticity, *Water Resour. Res.*, 50(3), 2350–2375,
972 doi:10.1002/2013WR014185, 2014.

973 Fernández-Martínez, M., Vicca, S., Janssens, I. A., Sardans, J., Luysaert, S., Campioli, M.,
974 Chapin III, F. S., Ciais, P., Malhi, Y., Obersteiner, M., Papale, D., Piao, S. L., Reichstein,
975 M., Rodà, F. and Peñuelas, J.: Nutrient availability as the key regulator of global forest
976 carbon balance, *Nat. Clim. Chang.*, 4, 471 [online] Available from:
977 <http://dx.doi.org/10.1038/nclimate2177>, 2014.

978 Gelman, A. and Rubin, D. B.: Inference from Iterative Simulation Using Multiple Sequences, *Stat.*
979 *Sci.*, 7(4), 457–472, doi:10.1214/ss/1177011136, 1992.

980 German, D. P., Marcelo, K. R. B., Stone, M. M. and Allison, S. D.: The Michaelis–Menten kinetics
981 of soil extracellular enzymes in response to temperature: a cross-latitudinal study, *Glob.*
982 *Chang. Biol.*, 18(4), 1468–1479, doi:10.1111/j.1365-2486.2011.02615.x, 2011.

983 Del Giudice, D., Honti, M., Scheidegger, A., Albert, C., Reichert, P. and Rieckermann, J.:
984 Improving uncertainty estimation in urban hydrological modeling by statistically
985 describing bias, *Hydrol. Earth Syst. Sci.*, 17(10), 4209–4225, doi:10.5194/hess-17-4209-
986 2013, 2013.

987 Gragne, A. S., Sharma, A., Mehrotra, R. and Alfredsen, K.: Improving real-time inflow forecasting
988 into hydropower reservoirs through a complementary modelling framework, *Hydrol. Earth*
989 *Syst. Sci.*, 19(8), 3695–3714, doi:10.5194/hess-19-3695-2015, 2015.

990 Hararuk, O., Xia, J. and Luo, Y.: Evaluation and improvement of a global land model against soil
991 carbon data using a Bayesian Markov chain Monte Carlo method, *J. Geophys. Res.*
992 *Biogeosciences*, 119(3), 403–417, doi:10.1002/2013JG002535, 2014.

993 Hashimoto, S., Morishita, T., Sakata, T., Ishizuka, S., Kaneko, S. and Takahashi, M.: Simple

994 models for soil CO₂, CH₄, and N₂O fluxes calibrated using a Bayesian approach and
995 multi-site data, *Ecol. Modell.*, 222(7), 1283–1292, doi:10.1016/j.ecolmodel.2011.01.013,
996 2011.

997 He, H., Meyer, A., Jansson, P., Svensson, M., Rütting, T. and Klemmedtsson, L.: Simulating
998 ectomycorrhiza in boreal forests : implementing ectomycorrhizal fungi model MYCOFON
999 in CoupModel (v5), *Geosci. Model Dev.*, 725–751, 2018.

1000 Hilton, T. W., Davis, K. J. and Keller, K.: Evaluating terrestrial CO₂flux diagnoses and
1001 uncertainties from a simple land surface model and its residuals, *Biogeosciences*, 11(2),
1002 217–235, doi:10.5194/bg-11-217-2014, 2014.

1003 Hoeting, J. A., Madigan, D., Raftery, A. E. and Volinsky, C. T.: Bayesian model averaging: a
1004 tutorial (with comments by M. Clyde, David Draper and E. I. George, and a rejoinder by
1005 the authors, *Stat. Sci.*, 14(4), 382–417, doi:10.1214/ss/1009212519, 1999.

1006 Högberg, P. and Read, D. J.: Towards a more plant physiological perspective on soil ecology,
1007 *Trends Ecol. Evol.*, 21(10), 548–554, doi:10.1016/j.tree.2006.06.004, 2006.

1008 Hublart, P., Ruelland, D., De Cortázar-Atauri, I. G., Gascoin, S., Lhermitte, S. and Ibacache, A.:
1009 Reliability of lumped hydrological modeling in a semi-arid mountainous catchment facing
1010 water-use changes, *Hydrol. Earth Syst. Sci.*, 20(9), 3691–3717, doi:10.5194/hess-20-3691-
1011 2016, 2016.

1012 Ishikura, K., Yamada, H., Toma, Y., Takakai, F., Darung, U., Limin, A. and Limin, S. H.: Soil
1013 Science and Plant Nutrition Effect of groundwater level fluctuation on soil respiration rate
1014 of tropical peatland in Central Kalimantan , Indonesia, *Soil Sci. Plant Nutr.*, 63(1), 1–13,
1015 doi:10.1080/00380768.2016.1244652, 2017.

1016 Janssens, I. A., Freibauer, A., Ciais, P., Smith, P., Nabuurs, G.-J., Folberth, G., Schlamadinger, B.,

1017 Hutjes, R. W. A., Ceulemans, R., Schulze, E.-D., Valentini, R. and Dolman, A. J.: Europe's
1018 terrestrial biosphere absorbs 7 to 12% of European anthropogenic CO₂ emissions.,
1019 Science, 300(5625), 1538–42, doi:10.1126/science.1083592, 2003.

1020 Katz, R. W., Craigmile, P. F., Guttorp, P., Haran, M., Sansó, B. and Stein, M. L.: Uncertainty
1021 analysis in climate change assessments, Nat. Clim. Chang., 3, 769 [online] Available from:
1022 <http://dx.doi.org/10.1038/nclimate1980>, 2013.

1023 Kavetski, D., Franks, S. W. and Kuczera, G.: Confronting Input Uncertainty in Environmental
1024 Modelling, Calibration Watershed Model., doi:doi:10.1029/WS006p0049, 2013.

1025 Keenan, T. F., Davidson, E., Moffat, A. M., Munger, W. and Richardson, A. D.: Using model-data
1026 fusion to interpret past trends, and quantify uncertainties in future projections, of terrestrial
1027 ecosystem carbon cycling, Glob. Chang. Biol., 18(8), 2555–2569, doi:10.1111/j.1365-
1028 2486.2012.02684.x, 2012.

1029 Kim, Y., Nishina, K., Chae, N., Park, S. J., Yoon, Y. J. and Lee, B. Y.: Constraint of soil moisture
1030 on CO₂ efflux from tundra lichen, moss, and tussock in Council, Alaska, using a
1031 hierarchical Bayesian model, Biogeosciences, 5567–5579, doi:10.5194/bg-11-5567-2014,
1032 2014.

1033 Klemedtsson, L., Jansson, P. E., Gustafsson, D., Karlberg, L., Weslien, P., Von Arnold, K.,
1034 Ernfors, M., Langvall, O. and Lindroth, A.: Bayesian calibration method used to elucidate
1035 carbon turnover in forest on drained organic soil, Biogeochemistry, 89(1), 61–79,
1036 doi:10.1007/s10533-007-9169-0, 2008.

1037 Laloy, E. and Vrugt, J. A.: High-dimensional posterior exploration of hydrologic models using
1038 multiple-try DREAM(ZS) and high-performance computing, Water Resour. Res., 48(1),
1039 doi:10.1029/2011WR010608, 2012.

1040 Li, J., Wang, G., Allison, S. D., Mayes, M. A. and Luo, Y.: Soil carbon sensitivity to temperature
1041 and carbon use efficiency compared across microbial-ecosystem models of varying
1042 complexity, *Biogeochemistry*, 119, 67–84 [online] Available from:
1043 <http://www.jstor.org/stable/24716883>, 2014.

1044 Li, M., Wang, Q. J., Bennett, J. C. and Robertson, D. E.: A strategy to overcome adverse effects
1045 of autoregressive updating of streamflow forecasts, *Hydrol. Earth Syst. Sci.*, 19(1), 1–15,
1046 doi:10.5194/hess-19-1-2015, 2015.

1047 Li, M., Wang, Q. J., Bennett, J. C. and Robertson, D. E.: Error reduction and representation in
1048 stages (ERRIS) in hydrological modelling for ensemble streamflow forecasting, *Hydrol.*
1049 *Earth Syst. Sci.*, 20(9), 3561–3579, doi:10.5194/hess-20-3561-2016, 2016a.

1050 Li, Q., Xia, J., Shi, Z., Huang, K., Du, Z. and Lin, G.: Variation of parameters in a Flux-Based
1051 Ecosystem Model across 12 sites of terrestrial ecosystems in the conterminous USA, *Ecol.*
1052 *Modell.*, 336, 57–69, doi:10.1016/j.ecolmodel.2016.05.016, 2016b.

1053 Lu, D., Ye, M., Meyer, P. D., Curtis, G. P., Shi, X., Niu, X.-F. and Yabusaki, S. B.: Effects of error
1054 covariance structure on estimation of model averaging weights and predictive performance,
1055 *Water Resour. Res.*, 49(9), 6029–6047, doi:10.1002/wrcr.20441, 2013.

1056 Luo, Y., Ogle, K., Tucker, C., Fei, S., Gao, C., LaDeau, S., Clark, J. S. and Schimel, D. S.:
1057 Ecological forecasting and data assimilation in a data-rich era, *Ecol. Appl.*, 21(5), 1429–
1058 1442, doi:10.1890/09-1275.1, 2011.

1059 Luo, Y., Keenan, T. F. and Smith, M.: Predictability of the terrestrial carbon cycle, *Glob. Chang.*
1060 *Biol.*, 21(5), 1737–1751, doi:10.1111/gcb.12766, 2014.

1061 Manzoni, S., Taylor, P., Richter, A., Porporato, A. and Ågren, G. I.: Environmental and
1062 stoichiometric controls on microbial carbon-use efficiency in soils, *New Phytol.*, 196(1),

1063 79–91, doi:10.1111/j.1469-8137.2012.04225.x, 2012.

1064 McInerney, D., Thyer, M., Kavetski, D., Lerat, J. and Kuczera, G.: Improving probabilistic
1065 prediction of daily streamflow by identifying Pareto optimal approaches for modeling
1066 heteroscedastic residual errors, *Water Resour. Res.*, 53, 2199–2239,
1067 doi:10.1002/2016WR019168.Received, 2017.

1068 Menichetti, L., Kätterer, T. and Leifeld, J.: Parametrization consequences of constraining soil
1069 organic matter models by total carbon and radiocarbon using long-term field data,
1070 *Biogeosciences*, 3003–3019, doi:10.5194/bg-13-3003-2016, 2016.

1071 Nash, J. E. and Sutcliffe, J. V: River flow forecasting through conceptual models part I — A
1072 discussion of principles, *J. Hydrol.*, 10(3), 282–290, doi:https://doi.org/10.1016/0022-
1073 1694(70)90255-6, 1970.

1074 Ogle, K., Ryan, E., Dijkstra, F. A. and Pendall, E.: *Journal of Geophysical Research:*
1075 *Biogeosciences*, *J. Geophys. Res. Biogeosciences*, 1–14, doi:10.1002/2016JG003385,
1076 2016.

1077 Pappenberger, F. and Beven, K. J.: Ignorance is bliss: Or seven reasons not to use uncertainty
1078 analysis, *Water Resour. Res.*, 42(5), doi:10.1029/2005WR004820, 2006.

1079 Peters, W., Jacobson, A. R., Sweeney, C., Andrews, A. E., Conway, T. J., Masarie, K., Miller, J.
1080 B., Bruhwiler, L. M. P., Pétron, G., Hirsch, A. I., Worthy, D. E. J., van der Werf, G. R.,
1081 Randerson, J. T., Wennberg, P. O., Krol, M. C. and Tans, P. P.: An atmospheric perspective
1082 on North American carbon dioxide exchange: CarbonTracker., *Proc. Natl. Acad. Sci. U. S.*
1083 *A.*, 104(48), 18925–30, doi:10.1073/pnas.0708986104, 2007.

1084 Le Quéré, C., Peters, G. P., Andres, R. J., Andrew, R. M., Boden, T. A., Ciais, P., Friedlingstein,
1085 P., Houghton, R. A., Marland, G., Moriarty, R., Sitch, S., Tans, P., Arneeth, A., Arvanitis,

1086 A., Bakker, D. C. E., Bopp, L., Canadell, J. G., Chini, L. P., Doney, S. C., Harper, A.,
1087 Harris, I., House, J. I., Jain, A. K., Jones, S. D., Kato, E., Keeling, R. F., Klein Goldewijk,
1088 K., Körtzinger, A., Koven, C., Lefèvre, N., Maignan, F., Omar, A., Ono, T., Park, G.-H.,
1089 Pfeil, B., Poulter, B., Raupach, M. R., Regnier, P., Rödenbeck, C., Saito, S., Schwinger, J.,
1090 Segschneider, J., Stocker, B. D., Takahashi, T., Tilbrook, B., van Heuven, S., Viovy, N.,
1091 Wanninkhof, R., Wiltshire, A. and Zaehle, S.: Global carbon budget 2013, *Earth Syst. Sci.*
1092 *Data*, 6(1), 235–263, doi:10.5194/essd-6-235-2014, 2014.

1093 Raich, J. W. J. J. W., Potter, C. S. C. and Bhagawati, D.: Interannual variability in global soil
1094 respiration, 1980-94, *Glob. Chang. Biol.*, 8, 800–812, doi:10.1046/j.1365-
1095 2486.2002.00511.x, 2002.

1096 Ren, X., He, H., Moore, D. J. P., Zhang, L., Liu, M., Li, F., Yu, G. and Wang, H.: Uncertainty
1097 analysis of modeled carbon and water fluxes in a subtropical coniferous plantation, *J.*
1098 *Geophys. Res. Biogeosciences*, 118(4), 1674–1688, doi:10.1002/2013JG002402, 2013.

1099 Ricciuto, D. M., King, A. W., Dragoni, D. and Post, W. M.: Parameter and prediction uncertainty
1100 in an optimized terrestrial carbon cycle model: Effects of constraining variables and data
1101 record length, *J. Geophys. Res. Biogeosciences*, 116(1), 1–17,
1102 doi:10.1029/2010JG001400, 2011.

1103 Richardson, A. D. and Hollinger, D. Y.: Statistical modeling of ecosystem respiration using eddy
1104 covariance data: Maximum likelihood parameter estimation, and Monte Carlo simulation
1105 of model and parameter uncertainty, applied to three simple models, *Agric. For. Meteorol.*,
1106 131(3–4), 191–208, doi:10.1016/j.agrformet.2005.05.008, 2005.

1107 Sadegh, M. and Vrugt, J. A.: Bridging the gap between GLUE and formal statistical approaches:
1108 Approximate Bayesian computation, *Hydrol. Earth Syst. Sci.*, 17(12), 4831–4850,

1109 doi:10.5194/hess-17-4831-2013, 2013.

1110 Scharnagl, B., Vrugt, J. A., Vereecken, H. and Herbst, M.: Inverse modelling of in situ soil water
1111 dynamics: Investigating the effect of different prior distributions of the soil hydraulic
1112 parameters, *Hydrol. Earth Syst. Sci.*, 15(10), 3043–3059, doi:10.5194/hess-15-3043-2011,
1113 2011.

1114 Schimel, J. P. and Weintraub, M. N.: The implications of exoenzyme activity on microbial carbon
1115 and nitrogen limitation in soil: a theoretical model, *Soil Biol. Biochem.*, 35(4), 549–563,
1116 doi:10.1016/S0038-0717(03)00015-4, 2003.

1117 Schmidt, M. W. I., Torn, M. S., Abiven, S., Dittmar, T., Guggenberger, G., Janssens, I. A., Kleber,
1118 M., Kögel-Knabner, I., Lehmann, J., Manning, D. A. C., Nannipieri, P., Rasse, D. P.,
1119 Weiner, S. and Trumbore, S. E.: Persistence of soil organic matter as an ecosystem
1120 property, *Nature*, 478(7367), 49–56, doi:10.1038/nature10386, 2011.

1121 Scholz, K., Hammerle, A., Hiltbrunner, E. and Wohlfahrt, G.: Analyzing the Effects of Growing
1122 Season Length on the Net Ecosystem Production of an Alpine Grassland Using Model –
1123 Data Fusion, *Ecosystems*, 21(5), 982–999, doi:10.1007/s10021-017-0201-5, 2018.

1124 Schoups, G. and Vrugt, J. A.: A formal likelihood function for parameter and predictive inference
1125 of hydrologic models with correlated, heteroscedastic, and non-Gaussian errors, *Water
1126 Resour. Res.*, 46(10), 1–17, doi:10.1029/2009WR008933, 2010.

1127 Scott, R. L., Jenerette, G. D., Potts, D. L. and Huxman, T. E.: Effects of seasonal drought on net
1128 carbon dioxide exchange from a woody-plant-encroached semiarid grassland, *J. Geophys.
1129 Res. Biogeosciences*, 114(4), doi:10.1029/2008JG000900, 2009.

1130 Shi, X., Ye, M., Curtis, G. P., Miller, G. L., Meyer, P. D., Kohler, M., Yabusaki, S. and Wu, J.:
1131 Assessment of parametric uncertainty for groundwater reactive transport modeling, *Water*

1132 Resour. Res., 50(5), 4416–4439, doi:10.1002/2013WR013755, 2014.

1133 Sinsabaugh, R. L., Manzoni, S., Moorhead, D. L. and Richter, A.: Carbon use efficiency of
1134 microbial communities: stoichiometry, methodology and modelling, *Ecol. Lett.*, 16(7),
1135 930–939, doi:10.1111/ele.12113, 2013.

1136 Smith, M. W., Bracken, L. J. and Cox, N. J.: Toward a dynamic representation of hydrological
1137 connectivity at the hillslope scale in semiarid areas, *Water Resour. Res.*, 46(12),
1138 doi:10.1029/2009WR008496, 2010a.

1139 Smith, T., Sharma, A., Marshall, L., Mehrotra, R. and Sisson, S.: Development of a formal
1140 likelihood function for improved Bayesian inference of ephemeral catchments, *Water*
1141 *Resour. Res.*, 46(12), 1–11, doi:10.1029/2010WR009514, 2010b.

1142 Smith, T., Marshall, L. and Sharma, A.: Modeling residual hydrologic errors with Bayesian
1143 inference, *J. Hydrol.*, 528, 29–37, doi:10.1016/j.jhydrol.2015.05.051, 2015.

1144 Spaaks, J. H. and Bouten, W.: Resolving structural errors in a spatially distributed hydrologic
1145 model using ensemble Kalman filter state updates, *Hydrol. Earth Syst. Sci.*, 17(9), 3455–
1146 3472, doi:10.5194/hess-17-3455-2013, 2013.

1147 Steinacher, M. and Joos, F.: Transient Earth system responses to cumulative carbon dioxide
1148 emissions: Linearities, uncertainties, and probabilities in an observation-constrained model
1149 ensemble, *Biogeosciences*, 13(4), 1071–1103, doi:10.5194/bg-13-1071-2016, 2016.

1150 Tang, J. and Riley, W. J.: Weaker soil carbon–climate feedbacks resulting from microbial and
1151 abiotic interactions, *Nat. Clim. Chang.*, 5, 56 [online] Available from:
1152 <http://dx.doi.org/10.1038/nclimate2438>, 2014.

1153 Tang, J. and Zhuang, Q.: A global sensitivity analysis and Bayesian inference framework for
1154 improving the parameter estimation and prediction of a process-based Terrestrial

1155 Ecosystem Model, *J. Geophys. Res. Atmos.*, 114(D15), doi:10.1029/2009JD011724, 2009.

1156 Thiemann, M., Trosset, M., Gupta, H. and Sorooshian, S.: Bayesian recursive parameter estimation
1157 for hydrologic models, *Water Resour. Res.*, 37(10), 2521–2535,
1158 doi:10.1029/2000WR900405, 2001.

1159 Thyer, M., Renard, B., Kavetski, D., Kuczera, G., Franks, S. W. and Srikanthan, S.: Critical
1160 evaluation of parameter consistency and predictive uncertainty in hydrological modeling:
1161 A case study using Bayesian total error analysis, *Water Resour. Res.*, 45(12), 1–22,
1162 doi:10.1029/2008WR006825, 2009.

1163 Tiedeman, C. R. and Green, C. T.: Effect of correlated observation error on parameters,
1164 predictions, and uncertainty, *Water Resour. Res.*, 49(10), 6339–6355,
1165 doi:10.1002/wrcr.20499, 2013.

1166 Tsai, F. T.-C. and Elshall, A. S.: Hierarchical Bayesian model averaging for hydrostratigraphic
1167 modeling: Uncertainty segregation and comparative evaluation, *Water Resour. Res.*, 49(9),
1168 doi:10.1002/wrcr.20428, 2013.

1169 Tucker, C. L., Bell, J., Pendall, E. and Ogle, K.: Does declining carbon-use efficiency explain
1170 thermal acclimation of soil respiration with warming?, *Glob. Chang. Biol.*, 252–263,
1171 doi:10.1111/gcb.12036, 2013.

1172 Tucker, C. L., Young, J. M., Williams, D. G. and Ogle, K.: Process-based isotope partitioning of
1173 winter soil respiration in a subalpine ecosystem reveals importance of rhizospheric
1174 respiration, *Biogeochemistry*, 121, 389–408 [online] Available from:
1175 <http://www.jstor.org/stable/24717586>, 2014.

1176 Tuomi, M., Vanhala, P., Karhu, K., Fritze, H. and Liski, J.: Heterotrophic soil respiration-
1177 Comparison of different models describing its temperature dependence, *Ecol. Modell.*,

1178 211(1–2), 182–190, doi:10.1016/j.ecolmodel.2007.09.003, 2008.

1179 Vargas, R., Carbone, M. S., Reichstein, M. and Baldocchi, D. D.: Frontiers and challenges in soil
1180 respiration research: from measurements to model-data integration, *Biogeochemistry*,
1181 102(1), 1–13, doi:10.1007/s10533-010-9462-1, 2011.

1182 Vrugt, J. A. and Ter Braak, C. J. F.: DREAM(D): An adaptive Markov Chain Monte Carlo
1183 simulation algorithm to solve discrete, noncontinuous, and combinatorial posterior
1184 parameter estimation problems, *Hydrol. Earth Syst. Sci.*, 15(12), 3701–3713,
1185 doi:10.5194/hess-15-3701-2011, 2011.

1186 Vrugt, J. A., ter Braak, C. J. F., Diks, C. G. H. and Schoups, G.: Hydrologic data assimilation using
1187 particle Markov chain Monte Carlo simulation: Theory, concepts and applications, *Adv.*
1188 *Water Resour.*, 51, 457–478, doi:10.1016/j.advwatres.2012.04.002, 2013.

1189 Wang, G., Post, W. M. and Mayes, M. A.: Development of microbial-enzyme-mediated
1190 decomposition model parameters through steady-state and dynamic analyses, *Ecol. Appl.*,
1191 23(1), 255–272, doi:10.1890/12-0681.1, 2013.

1192 Weijs, S. V., Schoups, G. and Van De Giesen, N.: Why hydrological predictions should be
1193 evaluated using information theory, *Hydrol. Earth Syst. Sci.*, 14(12), 2545–2558,
1194 doi:10.5194/hess-14-2545-2010, 2010.

1195 Westerberg, I. K., Guerrero, J. L., Younger, P. M., Beven, K. J., Seibert, J., Halldin, S., Freer, J.
1196 E. and Xu, C. Y.: Calibration of hydrological models using flow-duration curves, *Hydrol.*
1197 *Earth Syst. Sci.*, 15(7), 2205–2227, doi:10.5194/hess-15-2205-2011, 2011.

1198 Wieder, W. R., Bonan, G. B. and Allison, S. D.: Global soil carbon projections are improved by
1199 modelling microbial processes, *Nat. Clim. Chang.*, 3, 909 [online] Available from:
1200 <http://dx.doi.org/10.1038/nclimate1951>, 2013.

1201 Wieder, W. R., Allison, S. D., Davidson, E. A., Georgiou, K., Hararuk, O., He, Y., Hopkins, F.,
1202 Luo, Y., Smith, M. J., Sulman, B., Todd-Brown, K., Wang, Y.-P., Xia, J. and Xu, X.:
1203 Explicitly representing soil microbial processes in Earth system models, *Global*
1204 *Biogeochem. Cycles*, 29(10), 1782–1800, doi:10.1002/2015GB005188, 2015.

1205 Van Wijk, M. T., Van Putten, B., Hollinger, D. Y. and Richardson, A. D.: Comparison of different
1206 objective functions for parameterization of simple respiration models, *J. Geophys. Res.*
1207 *Biogeosciences*, 113(3), 1–11, doi:10.1029/2007JG000643, 2008.

1208 Xu, T., White, L., Hui, D. and Luo, Y.: Probabilistic inversion of a terrestrial ecosystem model:
1209 Analysis of uncertainty in parameter estimation and model prediction, *Global Biogeochem.*
1210 *Cycles*, 20(2), 1–15, doi:10.1029/2005GB002468, 2006.

1211 Xu, X., Schimel, J. P., Thornton, P. E., Song, X., Yuan, F. and Goswami, S.: Substrate and
1212 environmental controls on microbial assimilation of soil organic carbon: a framework for
1213 Earth system models, *Ecol. Lett.*, 17(5), 547–555, doi:10.1111/ele.12254, 2014.

1214 Yeluripati, J. B., van Oijen, M., Wattenbach, M., Neftel, A., Ammann, A., Parton, W. J. and Smith,
1215 P.: Bayesian calibration as a tool for initialising the carbon pools of dynamic soil models,
1216 *Soil Biol. Biochem.*, 41(12), 2579–2583, doi:10.1016/j.soilbio.2009.08.021, 2009.

1217 Yuan, W., Liang, S., Liu, S., Weng, E., Luo, Y. and Hollinger, D.: Improving model parameter
1218 estimation using coupling relationships between vegetation production and ecosystem
1219 respiration, *Ecol. Modell.*, 240, 29–40, doi:10.1016/j.ecolmodel.2012.04.027, 2012.

1220 Yuan, W., Xu, W., Ma, M., Chen, S. and Liu, W.: Agricultural and Forest Meteorology Improved
1221 snow cover model in terrestrial ecosystem models over the Qinghai – Tibetan Plateau,
1222 *Agric. For. Meteorol.*, 218–219, 161–170, doi:10.1016/j.agrformet.2015.12.004, 2016.

1223 Zhang, X., Niu, G.-Y., Elshall, A. S., Ye, M., Barron-Gafford, G. A. and Pavao-Zuckerman, M.:

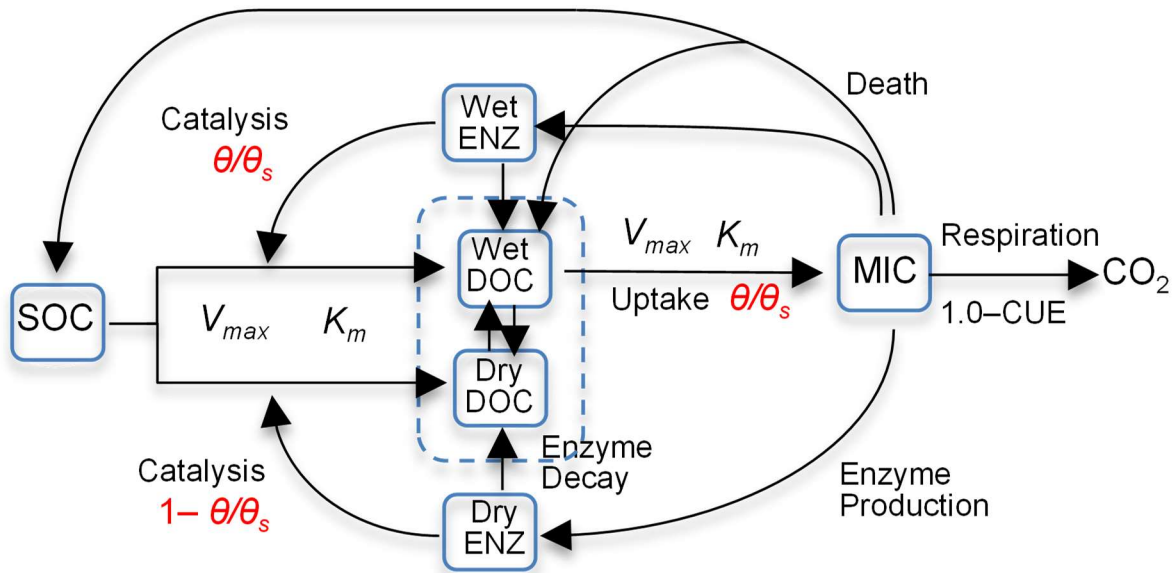
1224 Assessing five evolving microbial enzyme models against field measurements from a
1225 semiarid savannah - What are the mechanisms of soil respiration pulses?, *Geophys. Res.*
1226 *Lett.*, 41(18), doi:10.1002/2014GL061399, 2014.

1227 Zhou, X., Luo, Y., Gao, C., Verburg, P. S. J., Arnone, J. A., Darrouzet-Nardi, A. and Schimel, D.
1228 S.: Concurrent and lagged impacts of an anomalously warm year on autotrophic and
1229 heterotrophic components of soil respiration: A deconvolution analysis, *New Phytol.*,
1230 187(1), 184–198, doi:10.1111/j.1469-8137.2010.03256.x, 2010.

1231

1232 Figure 1. Diagram of model 6C representing the processes of (1) degradation of soil organic carbon
 1233 (SOC) to dissolved organic carbon (DOC) through catalysis of enzymes (ENZ) produced by
 1234 microbes (MIC), (2) MIC uptake of DOC, and (3) microbial (MIC) respiration to produce CO₂
 1235 (CUE is the carbon use efficiency). SOC degradation and microbial uptake rates are controlled by
 1236 water saturation (θ / θ_s). The DOC and ENZ pools are split into two subpools, one for the wet zone
 1237 and the other for the dry zone of the soil pore space. Microbial uptake of DOC occurs only in the
 1238 wet zone, and the uptake rate is linearly related to θ / θ_s . Catalysis through ENZ in the wet zone is
 1239 proportional to θ / θ_s , while that in the dry zone is proportional to $1 - \theta / \theta_s$. V_{max} (s⁻¹) is the maximum
 1240 rate, and K_m is the half-saturation concentration.

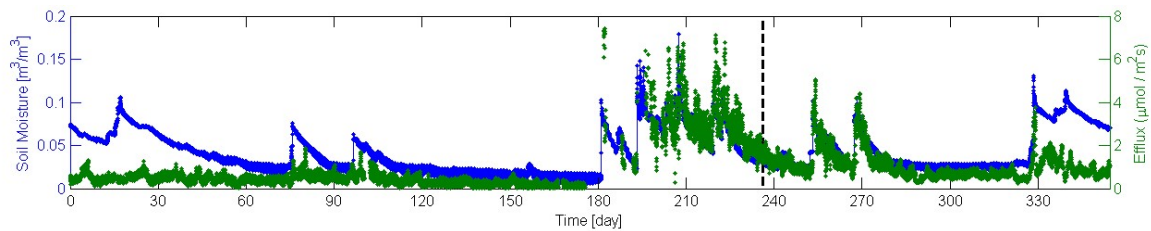
1241



1242

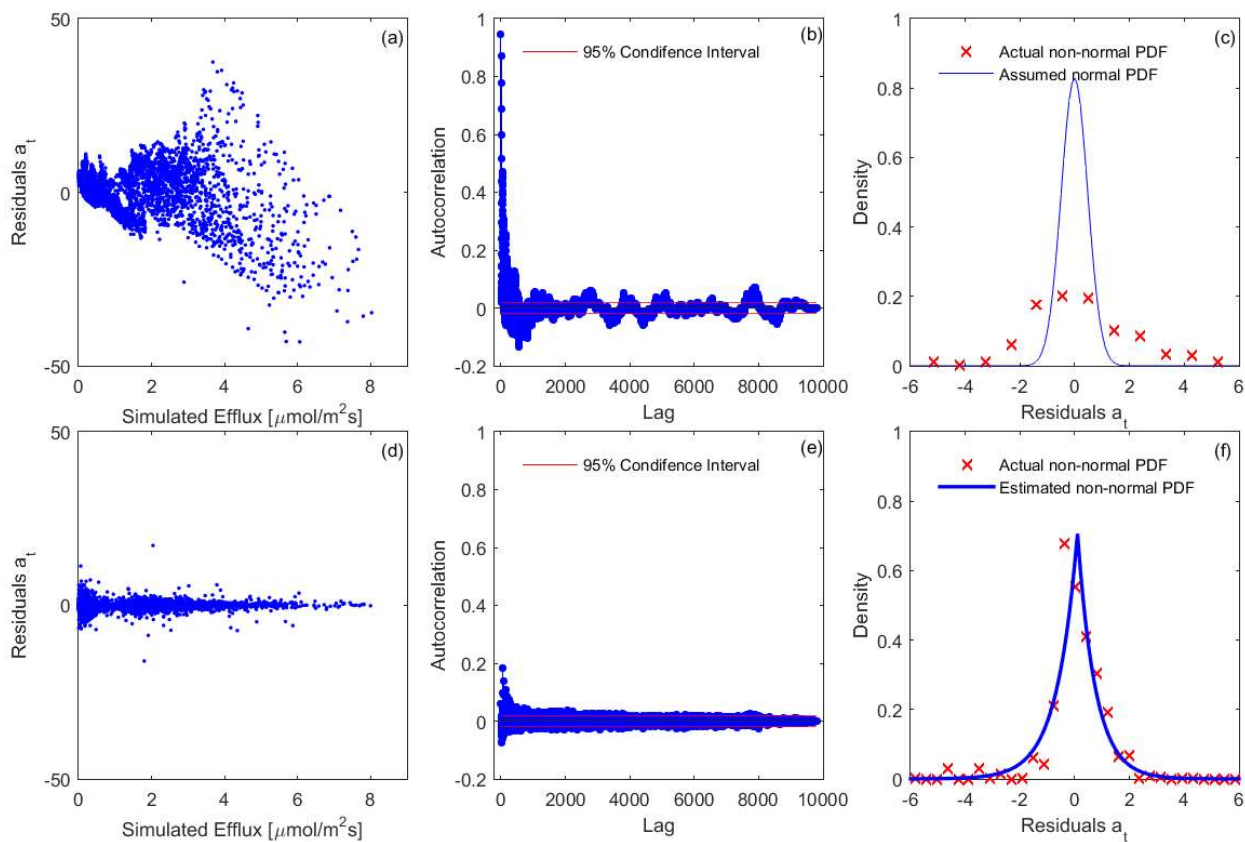
1243

1244 Figure 2. Time series of soil moisture and efflux observations. The dashed line marks the divide
1245 of the dataset into calibration and validation periods.
1246



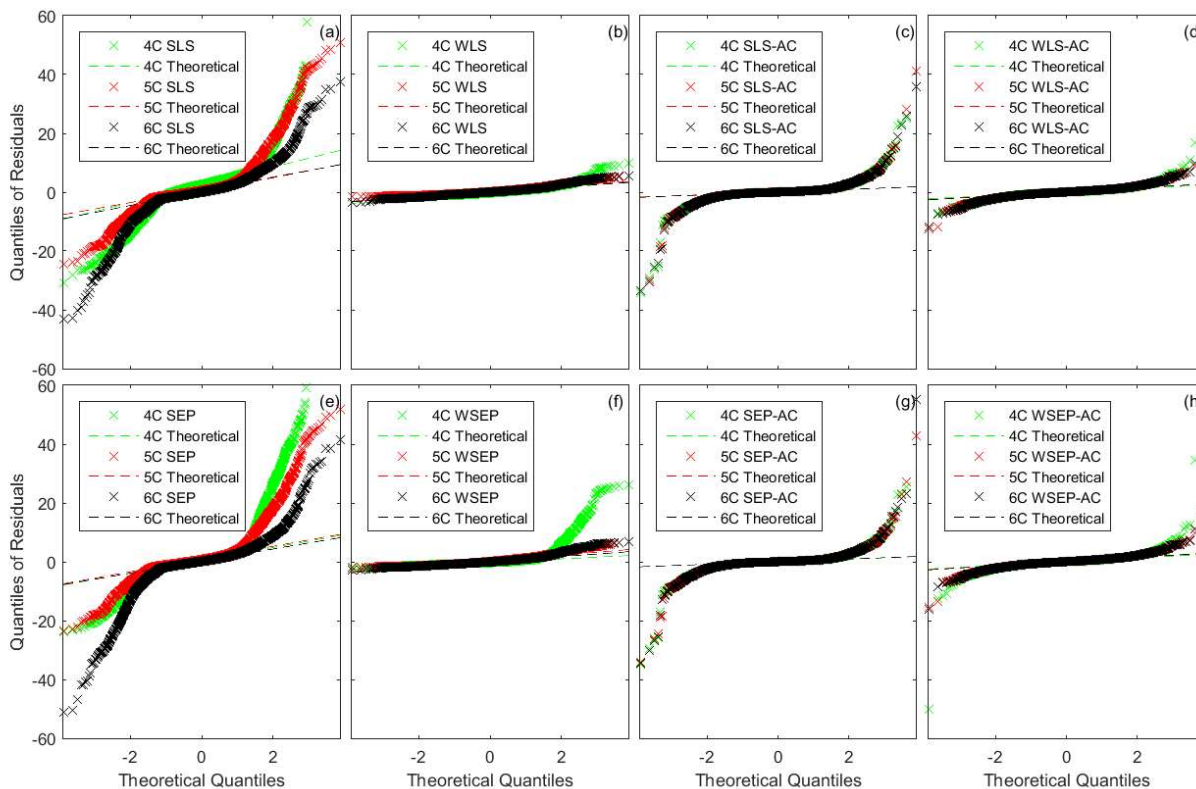
1247

1248 Figure 3. Residual analysis of the best realization (among multiple MCMC realizations) for model
1249 6C using data models (a-c) SLS and (d-f) WSEP-AC.
1250



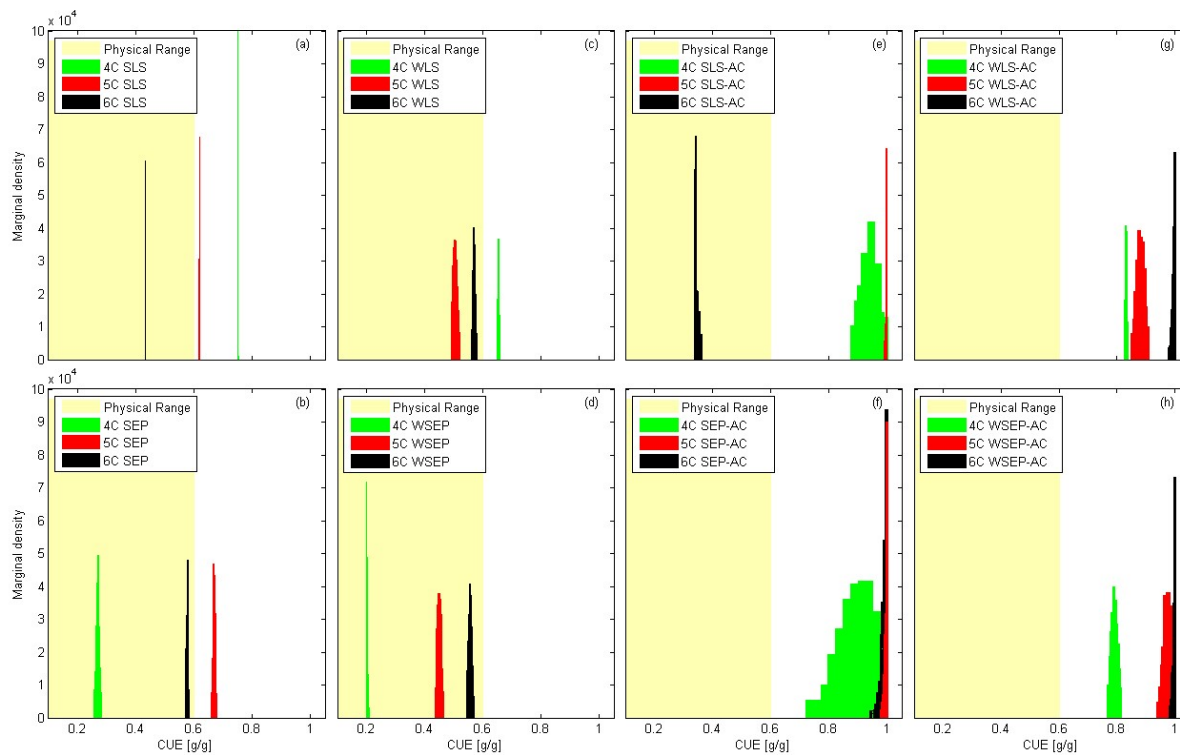
1251

1252 Figure 4. Residual quantile-quantile (Q-Q) plots of the best realization (among multiple MCMC
1253 realizations) for the three soil respiration models and eight data models.
1254



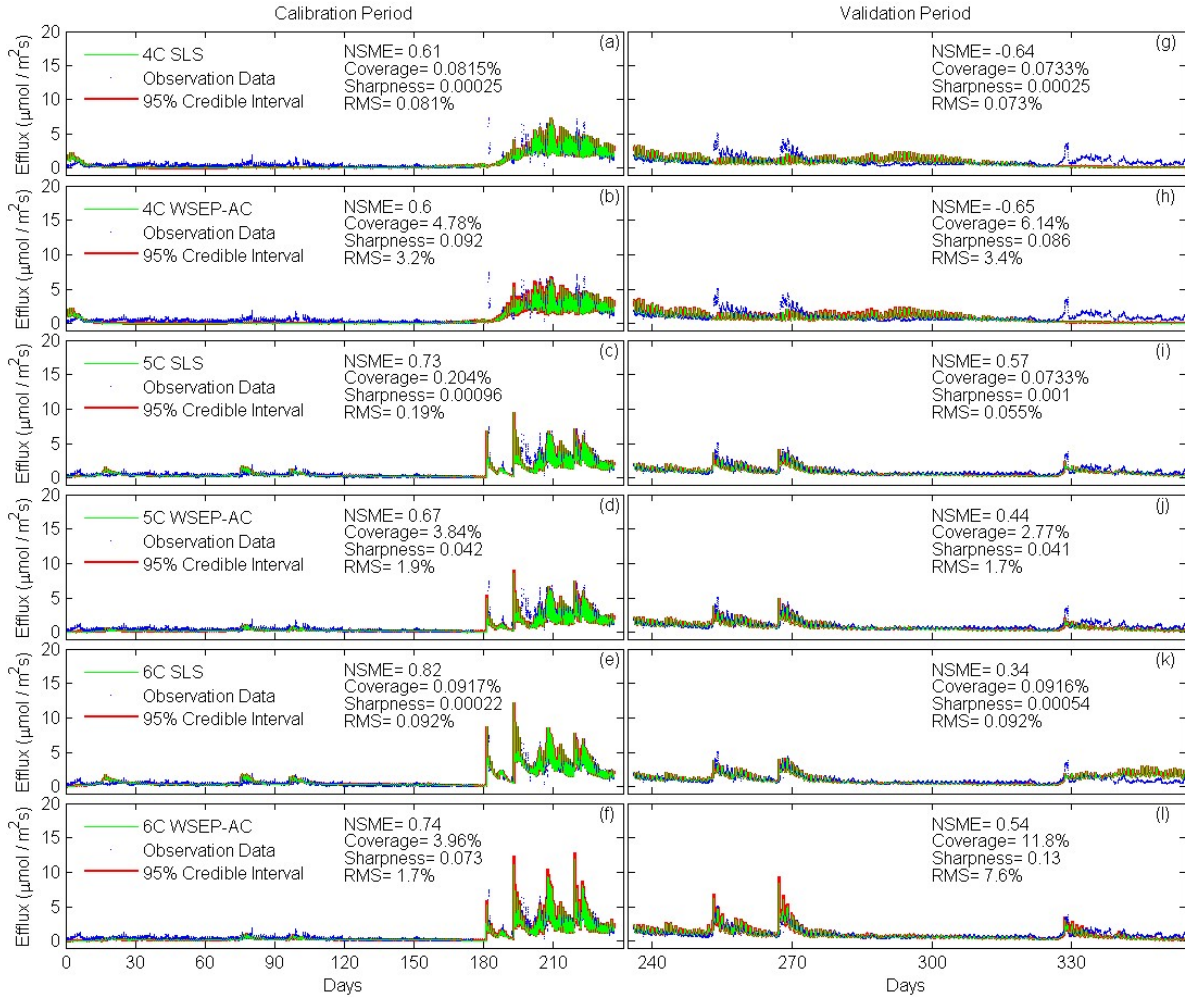
1255

1256 Figure 5. Marginal posterior parameter density of carbon use efficiency (CUE) for the three soil
 1257 respiration models and eight data models.
 1258



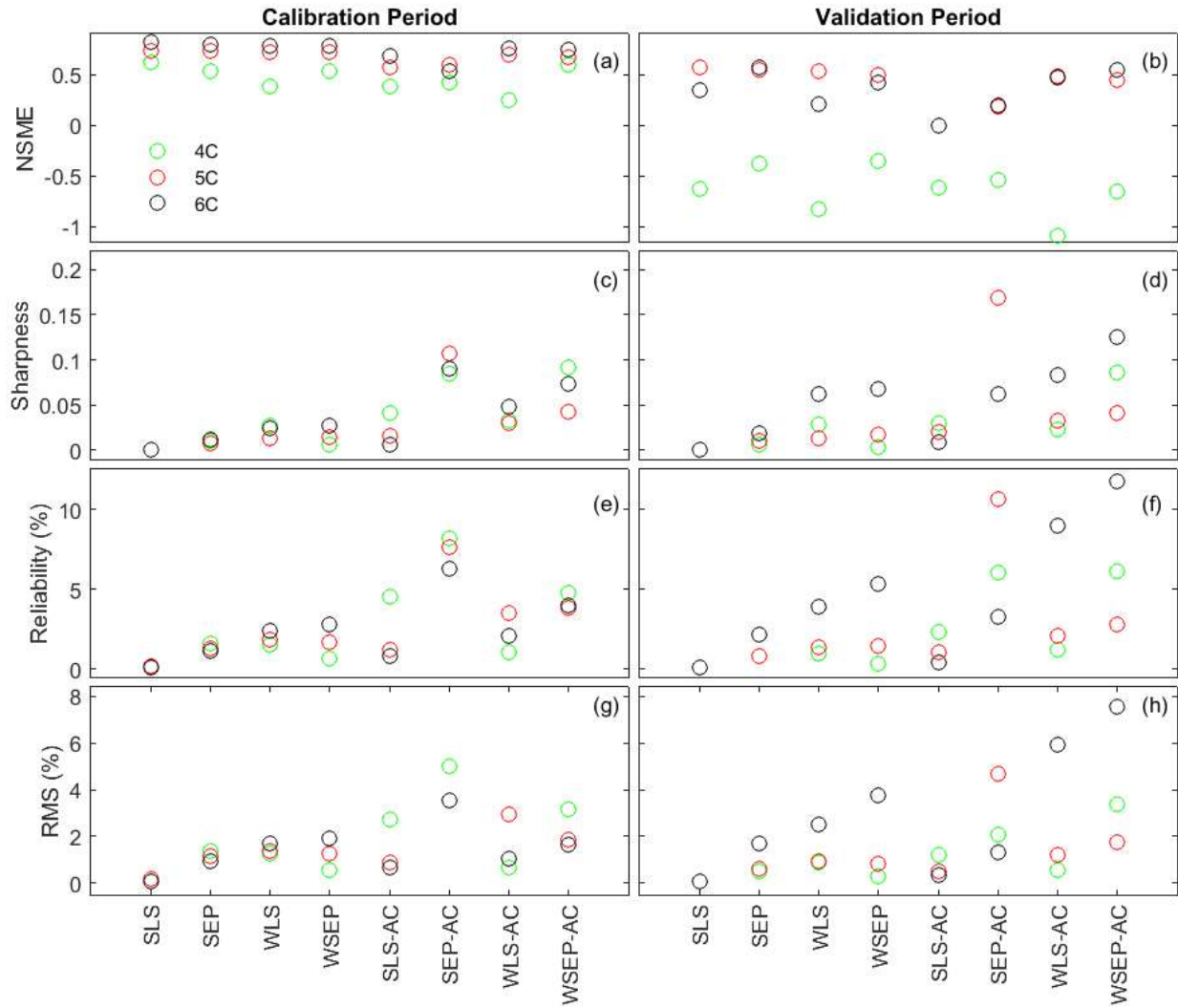
1259

1260 Figure 6. Observation data (blue dots) and mean prediction (green line) and 95% credible intervals
 1261 (red line) of prediction ensembles for (a)-(f) the calibration period and (g)-(l) the validation period.
 1262 The plots are for the three soil respiration models using data models SLS and WSEP-AC. *The*
 1263 *prediction ensembles are generated to consider parametric uncertainty of the soil respiration*
 1264 *models only.*
 1265



1266

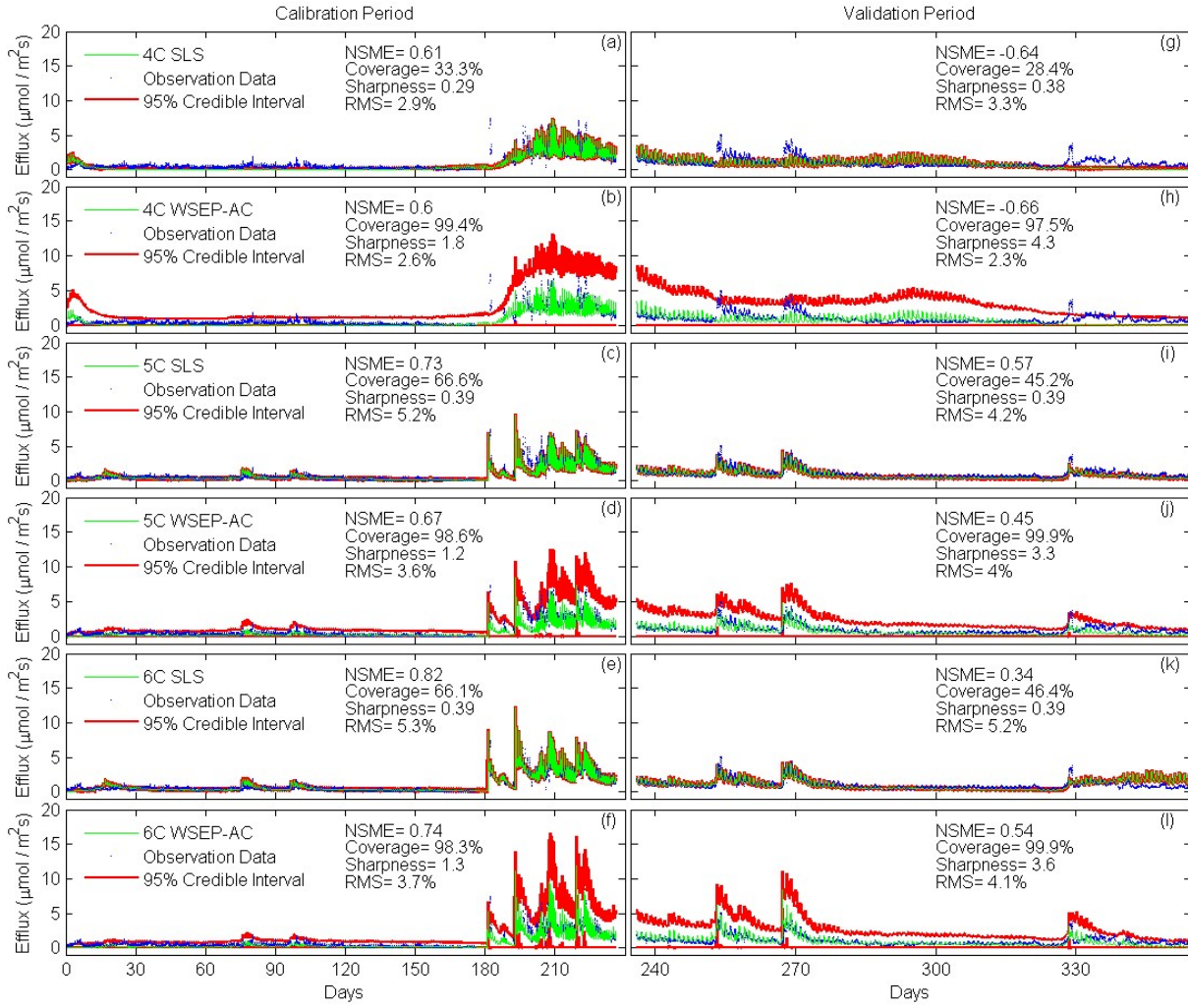
1267 Figure 7. (a-b) Nash-Sutcliffe model efficiency (NSME), (c)-(d) sharpness, (e)-(f) predictive
 1268 coverage, and (g)-(h) relative model score for measuring predictive performance of the three soil
 1269 respiration models and the eight data models during the calibration and cross-validation periods.
 1270 *The statistics are evaluated from the prediction ensembles generated to consider parametric*
 1271 *uncertainty of the soil respiration models only.*
 1272



1273

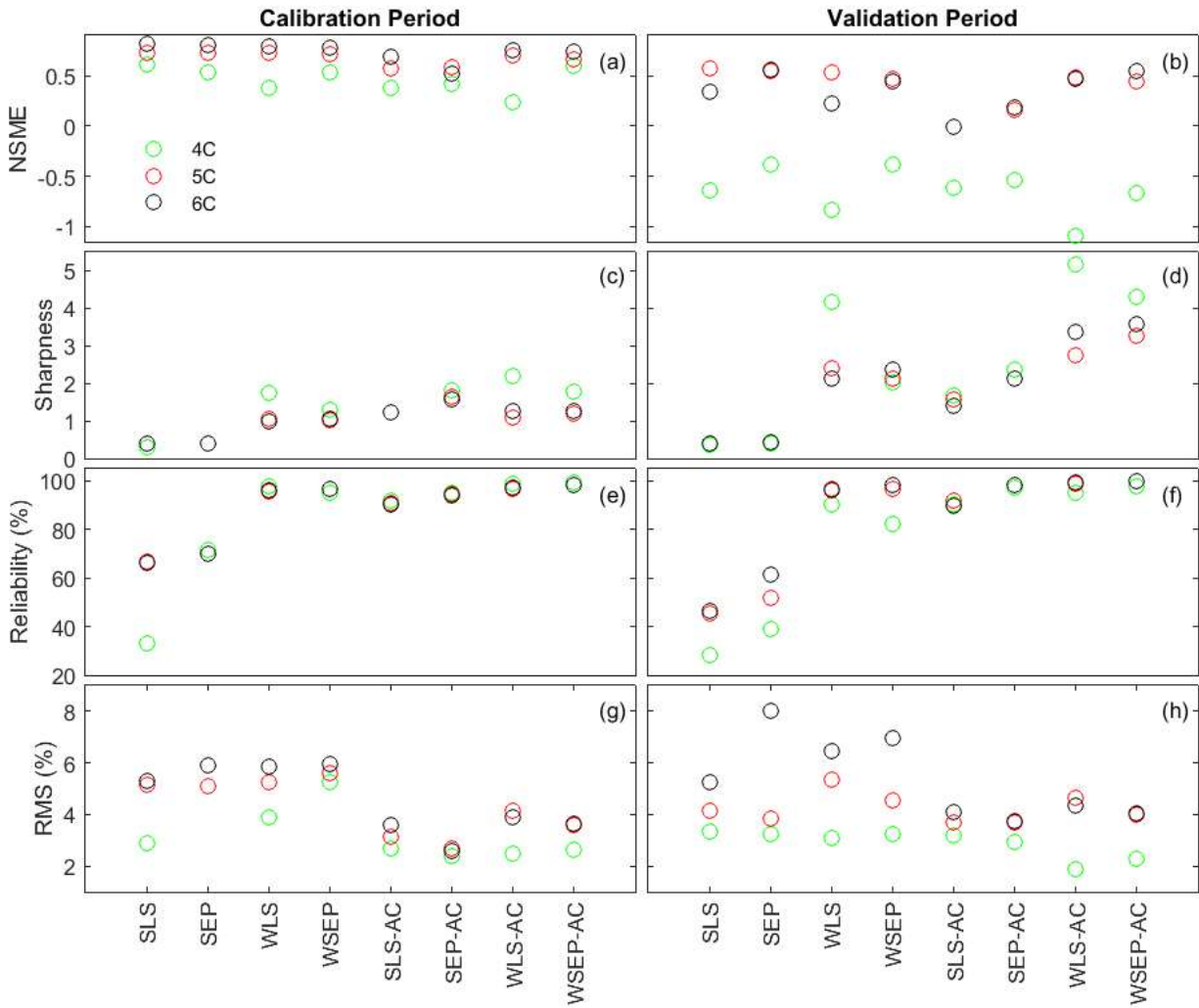
1274

1275 Figure 8. Observation data (blue dots) and mean prediction (green line) and 95% credible intervals
 1276 (red line) of prediction ensembles for (a)-(f) the calibration period and (g)-(l) the validation period.
 1277 The plots are for the three soil respiration models using data models SLS and WSEP-AC. *The*
 1278 *prediction ensembles are generated to consider parametric uncertainty of not only the soil*
 1279 *respiration models but also the data models.*
 1280



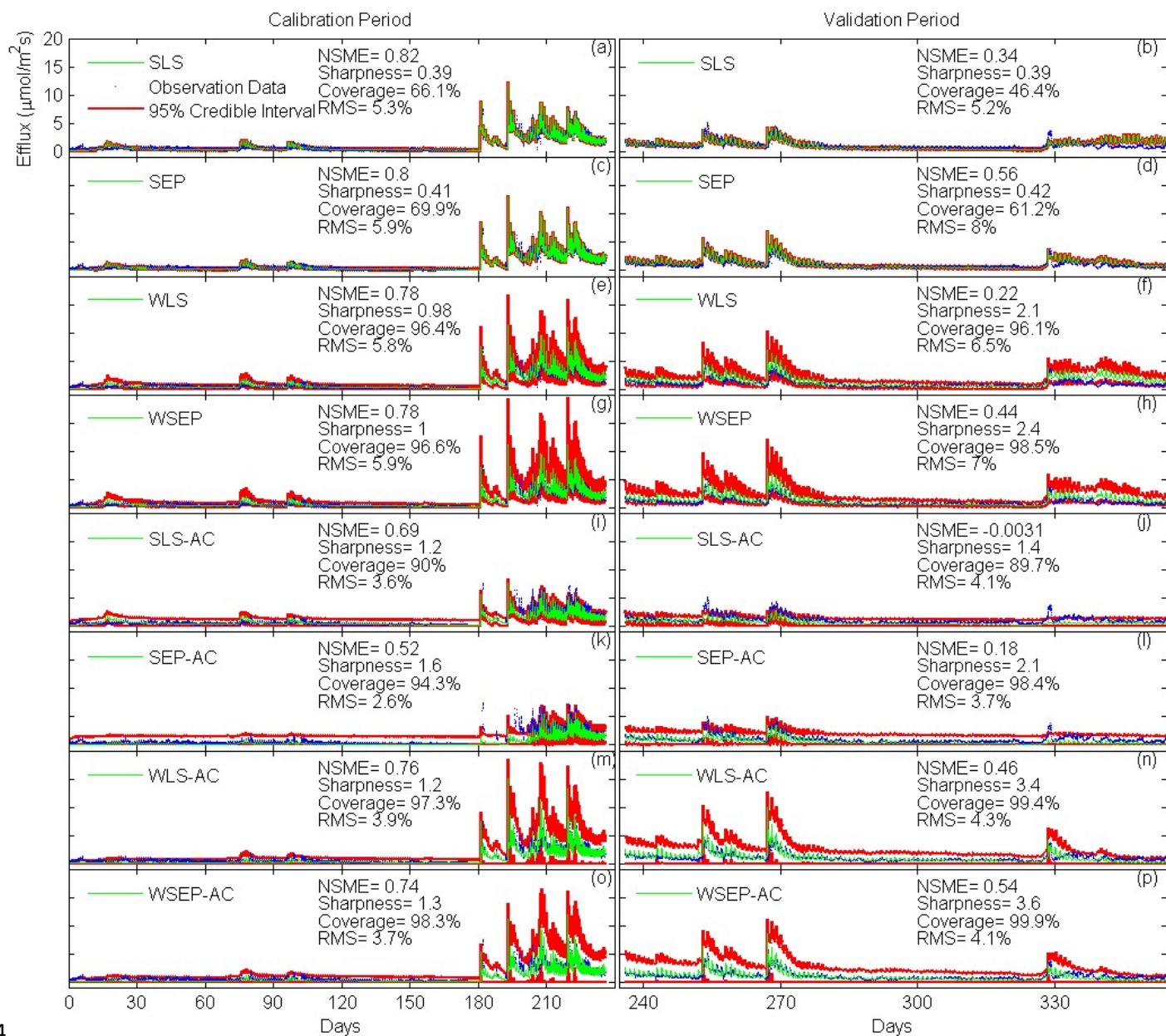
1281

1282 Figure 9. (a-b) Nash-Sutcliffe model efficiency (NSME), (c)-(d) sharpness, (e)-(f) predictive
 1283 coverage, and (g)-(h) relative model score for measuring predictive performance of the three soil
 1284 respiration models and the eight data models during the calibration and cross-validation periods.
 1285 *The statistics are evaluated from the prediction ensembles generated to consider parametric*
 1286 *uncertainty of not only the soil respiration models but also the data models.*
 1287



1288

1289 Figure 10. Observation data (blue dots) and mean prediction (green line) and 95% credible
 1290 intervals (red line) for 6C for the eight likelihood functions during the calibration period (a)-(h)
 1291 and the validation period (i)-(p). The prediction ensembles are generated to consider parametric
 1292 uncertainty of not only the soil respiration models but also the data models.
 1293



1294